END
DATE
FILMED
2-82
DTIC

MICROCOPY RESOLUTION TEST CHART
NATIONAL BUREAU OF STANDARDS 1963 A

| REPORT DOCUMENTATION PAGE | | READ INSTRUCTIONS BEFORE COMPLETING FORM |
|---|---|---|
| 1. REPORT NUMBER | 2. GOVT ACCESSION NO. | 3. RECIPIENT'S CATALOG NUMBER |
| 4. TITLE (and Subtitle)<br><br>PREDICTION OF SURF ZONE CHARACTERISTICS | | 5. TYPE OF REPORT & PERIOD COVERED<br>FINAL REPORT 1979-1981 |
| | | 6. PERFORMING ORG. REPORT NUMBER |
| 7. AUTHOR(s)<br><br>Joseph N. Suhayda<br>Gerald F. McHugh | | 8. CONTRACT OR GRANT NUMBER(s)<br><br>N00014-79-C-0342 |
| 9. PERFORMING ORGANIZATION NAME AND ADDRESS<br><br>Department of Civil Engineering<br>Louisiana State Unversity<br>Baton Rouge , LA 70803 | | 10. PROGRAM ELEMENT, PROJECT, TASK AREA & WORK UNIT NUMBERS<br><br>ONR Code 422 (CS) |
| 11. CONTROLLING OFFICE NAME AND ADDRESS<br><br>Office of Naval Research, Coastal Sciences Prog.<br>Code 422 (CS)<br>Arlington, Virginia 22217 | | 12. REPORT DATE<br>4 July 1981 |
| | | 13. NUMBER OF PAGES<br>66 |
| 14. MONITORING AGENCY NAME & ADDRESS(if different from Controlling Office) | | 15. SECURITY CLASS. (of this report)<br><br>Unclassified |
| | | 15a. DECLASSIFICATION/DOWNGRADING SCHEDULE |

16. DISTRIBUTION STATEMENT (of this Report)

Approved for public release, distribution unlimited

17. DISTRIBUTION STATEMENT (of the abstract entered in Block 20, if different from Report)

18. SUPPLEMENTARY NOTES

DEC 2 9 1981

19. KEY WORDS (Continue on reverse side if necessary and identify by block number)

Numerical Models
Breaker Heights

A

20. ABSTRACT (Continue on reverse side if necessary and identify by block number)

This report presents the results of the development and testing of predictive models for computing surf zone characteristics from wave measurements made outside the surf zone. The surf zone characteristics predicted are average breaker height, maximum breaker height, average breaker position, maximum breaker position, breaker type, average longshore current and maximum longshore current. Preliminary field tests indicate breaker height prediction was within ± 10 % for wave heights of about 1 meter.

DD FORM 1473 EDITION OF 1 NOV 65 IS OBSOLETE
1 JAN 73
S/N 0102-LF-014-6601

PREDICTION OF SURF ZONE CHARACTERISTICS

by

JOSEPH N. SUHAYDA and GERALD F. MCHUGH
DEPARTMENT OF CIVIL ENGINEERING
LOUISIANA STATE UNIVERSITY

July, 1980

# PREFACE

This report presents the results of studies conducted by the
Department of Civil Engineering, Louisiana State University, to support
the development of instruments for measuring waves and sediments in the
coastal zone. The research was conducted in cooperation with the Naval
Coastal Systems Center and with Dynex Consulting Company.

A

CONTENTS

# I. INTRODUCTION

This report presents the results of progress in the development of a predictive scheme for computing breaker characteristics from wave measurements outside the surf zone. This research was conducted in conjunction with an instrument development program of the Naval Coastal Systems Center. The NCSC program is aimed at improving UDT/SEAL reconnaisance through the development of a operational instrument package which will provide insitu data needed to determine the "effective surf" (1) at a beach site.

The objective of this study was to synthesize existing knowledge about breakers and surf and develop predictive models to be used with the NCSC or similar instruments. A secondary objective was to determine the usefulness of a penetrometer for measuring marine sediment properties.

The NCSC instrument will provide a time history of hydrodynamic pressure and the two horizontal components of the current at a point seaward of the breaker and surf zone. This type of data represents the boundary condition for surf zone wave processes. The problem is to develop a scheme for using boundary value data from offshore instruments with the aid of either a mini-computer (HP 9825 or HP 9830) or a large computer (IBM 3033) to compute surf zone parameters such as:

1) Average breaker height $(\overline{H})$ and maximum breaker height $(H_M)$.

2) Average breaker position $(\overline{X})$ and maximum breaker position $(X_M)$.

3) Breaker type.

4) Average longshore current $(V_1)$ and maximum longshore current $(V_{1M})$.

To be of engineering use, these parameters should be predicted within $\pm$10% for breaking waves up to a maximum height of 10 feet and $\pm$20% for large waves.

## II. ANALYTIC PREDICTION MODEL

The wave theory used for the analytic predictive model is linear wave theory. This theory is able to treat waves in intermediate and shallow water and is easily programmable onto a mini-computer. It is, of course, limited to waves of small height to wave length ratios (low steepness) and small wave height to water depth ratios. It is used in this predictive scheme as an initial step in the development of the model/instrument system.

It is assumed that a general bathymetric chart (or a UDT nearshore hydrographic survey chart (NHSC) (2)) is available for the beach site. A second assumption is that the instrument is placed at a known distance off the bottom ($d_i$) and that the current meter is oriented so that the component axes are parallel (y direction) and perpendicular (x direction) to the shoreline (see Figure 1). It is further assumed that the instrument outputs are sampled at a constant time interval, $\Delta t$, over an interval of time, T, to produce N data samples, where N equals $T/\Delta t$. Usually T will be in the range of 5 to 20 minutes and $\Delta t$ will be .25 to 1 sec.

### 1. Preliminary Computations

The preliminary computations include determining the mean pressure $(\overline{P})$, the pressure change between wave crest and wave trough for each wave ($\Delta P_j$, $j=1,\ldots,M$), the wave period for each wave ($T_j$), the mean velocity components ($\overline{V}$ and $\overline{U}$) and the wave crest current components ($U_{cj}$ and $V_{cj}$).

The wave parameters computed for the location of the instrument are:
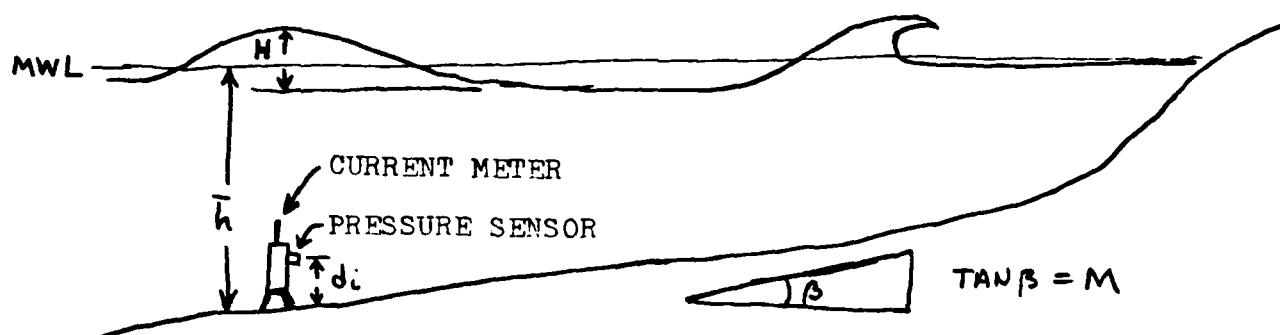
A. BEACH PROFILE
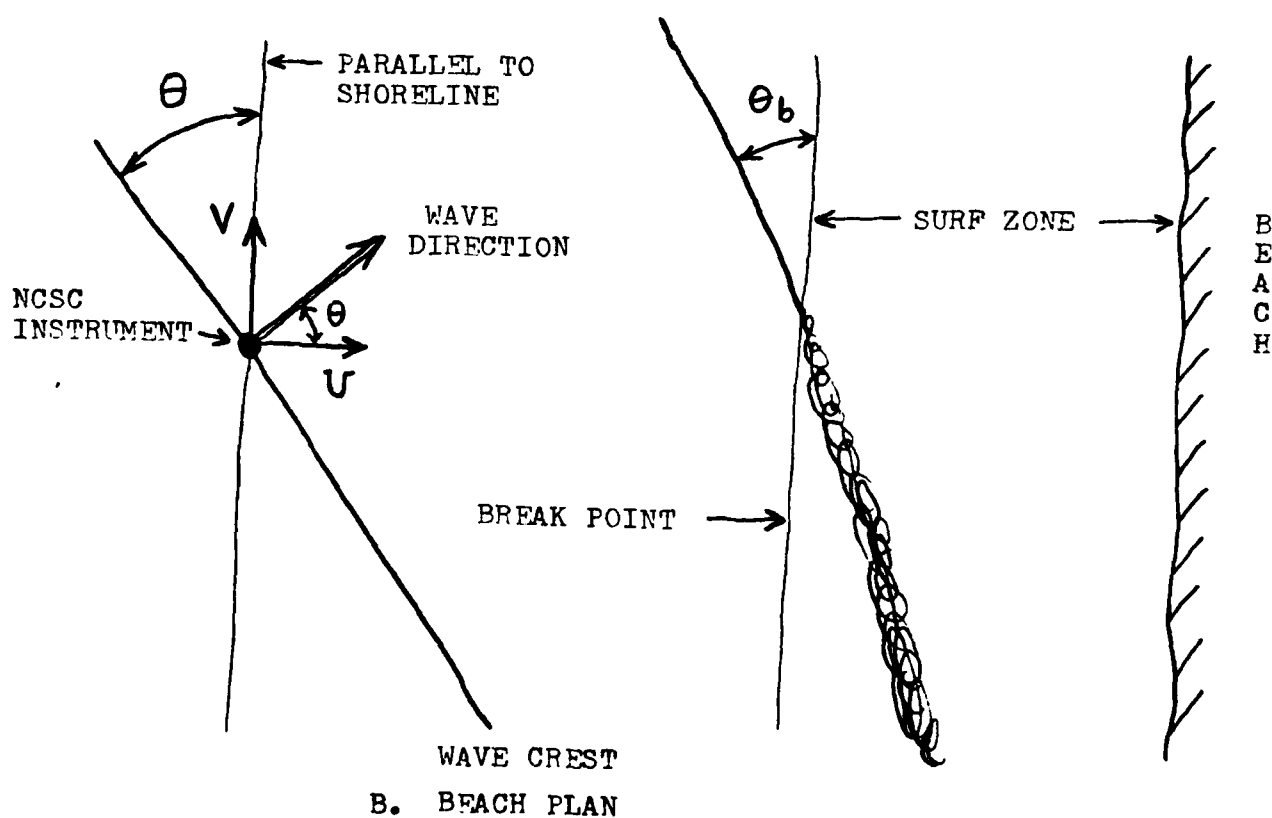
B. BEACH PLAN

Figure 1. Schematic diagram of beach and definition of variables.

water depth $\quad h = \dfrac{\overline{P}}{\mathfrak{s}\mathfrak{g}} + d_i$

and for each wave:

wave height $\quad H_j = \dfrac{\Delta P_j}{\mathfrak{s}\mathfrak{g}} \cdot \dfrac{\cosh(2\pi h/L_j)}{\cosh(2\pi d_i/L_j)}$

wave length $\quad \dfrac{2\pi}{T_j} = \dfrac{2\pi g}{L_j} \cdot \tanh(2\pi h/L_j)$

wave angle $\quad \theta_j = \tan^{-1}\left(\dfrac{Vc_j}{Uc_j}\right)$

## 2. Predictive Equations

The prediction of the surf zone parameters involves a set of equations which must be applied simultaneously. The equations use the instrument site wave parameters $H_j$, $T_j$, $L_j$, and $\theta_j$ to predict the same parameters at the break point $H_b$, $T_b$, $L_b$, $\theta_b$. It is assumed that the period of each wave remains constant so that $T_j = T_{bj}$. The equations are as follows (3):

1) Breaker Depth $\quad h_{bj} = H_{bj}(1 - 4.7m + 12m^2) \qquad m \leq .15$

2) Breaker Angle $\quad \sin\theta_{bj} = \dfrac{C_{bj}}{C_j}\sin\theta_j$

$$C_j = \dfrac{L_j}{T_j} \quad , \quad C_{bj} = \left[g(H_{bj} + h_{bj})\right]^{1/2}$$

3) Breaker Wavelength $\quad L_{bj} = C_{bj} \cdot T_{bj}$

4) Breaker Height $\quad H_{bj} = H_j \cdot K_{fj} \cdot K_{rj} \cdot K_{sj}$

where $\quad K_{rj} = .98 \quad , \quad K_{rj} = \left[ \dfrac{\cos \Theta_j}{\cos \Theta_{bj}} \right]^{1/2}$

$$K_{sj} = \left[ \left( \frac{TANH\,(2\pi h/L_j)}{TANH\,(2\pi h_{bj}/L_{bj})} \right) \cdot \frac{\left(1 + \dfrac{4\pi h/L_j}{SINH\,(4\pi h/L_j)}\right)}{\left(1 + \dfrac{4\pi b_{bj}/L_{bj}}{SINH\,(4\pi h_{bj}/L_{bj})}\right)} \right]$$

The set of breaker values are computed for $j = 1,,,,M$. For this the maximum breaker height $H_M$ can be identified, furthermore

$$\overline{H}_b = \frac{1}{M} \sum_{j=1}^{M} H_{bj} \quad , \quad \overline{h}_b = \frac{1}{M} \sum_{j=1}^{M} h_{bj}$$

$$\overline{\Theta}_b = \frac{1}{M} \sum_{j=1}^{M} \Theta_{bj}$$

The positions of $h_b$ and $h_{MAX}$ can be located on the nearshore chart.

The simultaneous solution of the set of equations needed to make a prediction is too complex for a practical scheme. Rather, the solution can be approximated by an interaction scheme in which initial values for selected parameters are computed from the input data. The formula for the initial value of the wave height is

$$H_{bj}^{*} = .95 \; h^{Y_5} \, H_j^{4/5}$$

With this initial value, the set of equations in the surf prediction model can be computed explicitly in order, that is, finding $h_{bj}$, use this to find $\Theta_{bj}$ and finally $H_{bj}$. The difference between $H_{bj}$ and $H_{bj}$ should be small (a few percent) and, it not, $H_{bj}$ can be used in place of $H_{bj}$ in a second iteration.

### 3. Breaker Type and Longshore Current

The prediction of breaker type is based upon breaker wave characteristics and the beach slope. The empirical formula suggested is:

$$\frac{H_{bj}}{L_{bj} \cdot m} > 1.2 \qquad \text{SPILLING BREAKER}$$

$$.5 \le \frac{H_{bj}}{L_{bj} \cdot m} \le 1.2 \qquad \text{PLUNGING BREAKER}$$

$$\frac{H_{bj}}{L_{bj} \cdot m} < .5 \qquad \text{SURGING BREAKER}$$

The prediction of longshore currents is based upon the theory for linear waves on a plane sloping beach. The formula for the maximum longshore current $V_m$ and the longshore current at the average breaker point $V_b$ are given by (4):

$$V_m = 20.7 \, m \left( g \bar{H}_b \right)^{1/2} \sin 2\bar{\theta}_b$$

and

$$V_b = .60 \, V_m$$

### 4. Verification

The analytic model presented in this report provides a means for making predictions of the desired surf parameters. The model is limited in application because of the assumptions contained in the underlying wave theory. The model does not account for wave induced pressure near the break point changes which differ from linear wave theory, resulting from wave crest accelerations (5). Furthermore the bottom topography is assumed to be planar and therefore real beach profiles and longshore bars cannot be treated. Finally, the longshore current predictions neglect temporal variations in current speed and spatial variations associated with nearshore topography.

Verification of the model accuracy has been attempted using the NCSC instrument, as reported at the Oceans 80 Conference (see Appendix 1 for reprint of article). The model predictions of average breaker heights (Table 1 of reprint) were about .10 to .15 meters too high for average breaker height of about 1 m. This could be accounted for by an increased frictioned attenuation coefficient ($K_F$).

5. References

(1) Department of the Navy, Joint PHIBPAC/PHIBLANT Surf Manual, COMPHIBLANTINST 3840.1F and COMPHIBPACINST 3840.3C, May, 1970.

(2) Department of the Navy, LST Beaching Reports and UDT Beach Survey Reports and Charts, COMPHIBGRUEASTPACINST 3820.1, February, 1976.

(3) U.S. Army Corps of Engineers Coastal Engineering Research Center, Shore Protection Manual, VOL I, II, and III, 1973.

(4) Longuet-Higgins, M. S., Longshore Currents Generated by Obliquely Indicent Sea Waves,1, J.G.R., 75,6778-6789, 1970.

(5) Van Dorn, W. G., Breaking Invariants in Shoaling Waves, J.G.R., 38(C6), pp 2981-2988.

## III. NUMERICAL PREDICTION MODEL

### 1. Introduction

Theoretical studies of gravity waves in incompressible fluids, begun in the early nineteenth century, have yielded predictive formulae of successively increasing accuracy. All of these analytical triu;?ᵗs suffer, however, from the common limitation of referring to physically simple geometric situations, in particular a wavefront moving over a plane bottom having a constant depth or slope. In order to obtain a solution to the general problem, we are compelled to introduce discretization of the space and time dimensions, and solve the governing equations for the dependent variables at all necessary points of the four-dimensional space-time grid. This means converting the analytic equations to finite-difference form.

However, the numerical problem posed by the general finite-difference equations is still formidable on account of its spatially three-dimensional character. In the simplest physical case of a homogeneous, isothermal, and incompressible fluid, there are four dependent variables: u, v, w, p--representing, respectively, the three components of velocity parallel to the coordinate axes x, y, z, and the pressure--to be calculated at every internal grid point, and the water level to be calculated at points in the horizontal plane. For nonisothermal or inhomogeneous liquids, two more dependent variables, the temperature and density must be added. In all applications to geographic situations where many wavelengths are involved (short wave propagation) the computer storage required is likely to be excessive. (At least ten grid

points are needed to define a wave profile). Thus the modeler will
probably find himself obliged to shrink the boundaries of his investiga-
tion to an insignificant size.

Given a viable grid, however, there still remains the problem of
specifiying realistic open water boundary values for all dependent
variables as a function of time, over the vertical plane.

A possible way out of these difficulties, and one which drastically
simplifies the numerical procedure, is to integrate the equations of
motion from bottom to surface and so remove one spatial dimension explicitly
from the problem. All dependent variables then need only be solved for
in the x-y plane.

The modeling of shallow water, or long waves (conventionally defined
as ones for which the wavelength exceeds twenty times the mean depth) by
means of vertically integrated equations, has received much attention.
Ever since Hansen (1956) introduced a viable finite-difference formulation
of these equations, numerous authors have applied his technique to
various seas, lakes, and bays. The long waves of interest to oceanographers
are principally those caused by the sun and moon (tides), and those
arising from strong winds and atmospheric fluctuations (storm surges).
Successful predictions of these phenomena have been obtained using the
Hansen equations solved explicitly, implicitly, or a mixture of both.

A desirable first approach to the solution of the general wave
problem in real geographic situations would be to apply the numerical
techniques already proven for solving the long wave equations. The
"general" wave equations would, however, need to retain a higher order
of validity. In obtaining soluble long-wave equations it has been
customary to make two simplifying assumptions: (1) that the horizontal

velocity vector is constant from bottom to surface, and (2) that the vertical acceleration is so small that the hydrostatic approximation is a good one. In the general case these restrictions would have to be relaxed.

To account for the unknown variability of the horizontal velocity component in the vertical direction, and a finite vertical acceleration, while keeping the problem amenable to a Hansen-type approach, requires the help of analytical, or closed-form solutions. These necessarily refer to the simplest geometric situation; but used in conjunction with the vertically integrated Navier-Stokes equations it is expected that they will allow a good first approximation to the solution of the general problem.

The recognition of a non-zero vertical acceleration in the fluid flow is tantamount to accepting a pressure distribution in the vertical deviating from the hydrostatic. Conversely, with a pressure distribution in the vertical taken from analytic or "zero order" theory, the vertical acceleration is implicitly accounted for.

## 2. Derivation of the Vertically Integrated Equations for the General Wave Problem

The three-dimensional, ensemble-averaged equations of motion for a homogeneous, incompressible fluid, with turbulent stresses on vertical planes and molecular viscous stresses neglected, can be written

$$\frac{\partial u}{\partial x} + \frac{\partial v}{\partial y} + \frac{\partial w}{\partial z} = 0$$

$$\frac{\partial u}{\partial t} + \frac{\partial u^2}{\partial x} + \frac{\partial uv}{\partial y} + \frac{\partial uw}{\partial z} - 2\Omega_z v = \frac{-1}{\rho}\frac{\partial p}{\partial x} - \frac{1}{\rho}\frac{\partial \tau_{xz}}{\partial z}$$

$$\frac{\partial v}{\partial t} + \frac{\partial vu}{\partial x} + \frac{\partial v^2}{\partial y} + \frac{\partial vw}{\partial z} + 2\Omega_z u = \frac{-1}{\rho}\frac{\partial p}{\partial y} - \frac{1}{\rho}\frac{\partial \tau_{vz}}{\partial z} \tag{1}$$

$$\frac{\partial w}{\partial t} + \frac{\partial wu}{\partial x} + \frac{\partial wv}{\partial y} + \frac{\partial w^2}{\partial z} + 2(\Omega_x v - \Omega_y u) = \frac{1}{\rho}\frac{\partial p}{\partial z} - g - \frac{1}{\rho}\frac{\partial \tau_{zz}}{\partial z}$$

where $\Omega$ is the earth's angular velocity vector, $\tau_{xz}$, $\tau_{yz}$, $\tau_{zz}$ are turbulent stress components on the horizontal plane in the directions x, y, z, respectively, g is the acceleration due to gravity; and other symbols have been defined. The Coriolis components of acceleration have been simplified by omission of terms involving w, on the assumption that $w \ll u, v$.

We eliminate the third momentum equation at the outset by adopting the pressure distribution from small amplitude, frictionless wave theory (see, for example Ippen (1966)):

$$p = -g\rho z + \frac{g\rho\cosh[k(h + z)]}{\cosh[kh]} \cdot \zeta \qquad (2)$$

In this equation the external, or atmospheric pressure is implicitly zero, and the origin of z (measured positively upward) is located at the still water surface. h is the depth of the bottom below this surface. The instantaneous height of the liquid surface relative to the plane z = 0, is $\zeta$. k is the wave number, defined by

$$k = 2\pi/L$$

where L is the wavelength. For the purpose of the ensuing analysis both k and h are considered — in contradistinction to linear theory — to be functions of x and y. Figure 1 illustrates the definitions of z, h and $\zeta$.

( See Figures Section of Report )

Fig. 1 Definition Diagram of z, h, and $\zeta$.

In the derivation of equation (2) the surface boundary condition was applied not at the actual surface z = $\zeta$, but at z = 0. Consequently, the equation has validity only from z = -h to z = 0. For positive z one must assume a hydrostatic pressure distribution.

Write $\quad \psi(z) = \dfrac{\cosh[k(h + z)]}{\cosh[kh]} \qquad -h \le z \le 0$ $\qquad\qquad$ (3)

$\psi$ has been termed the "pressure response factor". From equations (2) and (3)

$$\frac{1}{\rho}\frac{\partial p}{\partial x} = g\psi\,\frac{\partial \zeta}{\partial x} \;,\; \frac{1}{\rho}\frac{\partial p}{\partial y} = g\psi\,\frac{\partial \zeta}{\partial y}$$

With the last two relations, and replacing $2\Omega_z$ by the Coriolis parameter f, the equations to be solved become

$$\frac{\partial u}{\partial x} + \frac{\partial v}{\partial y} + \frac{\partial w}{\partial z}$$

$$\frac{\partial u}{\partial t} + \frac{\partial u^2}{\partial x} + \frac{\partial uv}{\partial y} + \frac{\partial uw}{\partial z} - fv = -g\psi\,\frac{\partial \zeta}{\partial x} - \frac{1}{\rho}\frac{\partial \tau_{xz}}{\partial z}$$

$$\frac{\partial v}{\partial t} + \frac{\partial vu}{\partial x} + \frac{\partial v^2}{\partial y} + \frac{\partial vw}{\partial z} + fu = -g\psi\,\frac{\partial \zeta}{\partial y} - \frac{1}{\rho}\frac{\partial \tau_{yz}}{\partial z}$$

$\qquad\qquad$ (4)

Equations (4) must be integrated over z between the limits $-$ h and $\zeta$. Consider firstly the integration of $\psi$. Here, in accordance with the previous remarks, the upper limit must be changed to z = 0. The error will not be serious if the small amplitude condition: $|\zeta| \ll h$ , holds. From equation (3)

$$\int_{-h}^{0} \psi\,dz = \frac{1}{k}\tanh[kh]$$

$\qquad\qquad$ (5)

Now, another result of the linear, or small amplitude theory is that

$$\sigma^2 = gk\,\tanh[kh]$$

$\qquad\qquad$ (6)

where $\sigma$ is the angular frequency of the wave, a constant. Eliminating tanh [kh] from equation (5) using equation (6), we then obtain approximately

$$\int_{-h}^{\zeta} g\psi\,\frac{\partial \zeta}{\partial x}\,dz = \frac{\sigma^2}{k^2}\frac{\partial \zeta}{\partial x}$$

$\qquad\qquad$ (7)

By definition of the phase speed, S

$$\frac{\sigma^2}{k^2} = S^2 \qquad (8)$$

For long waves, when $\psi = 1$ is a good approximation, the right hand side of equation (7) is replaced by

$$g(\zeta + h) \frac{\partial \zeta}{\partial x}$$

Boundary conditions that must be employed in the vertical integrations are:

$$\frac{\partial \zeta}{\partial t} + u\frac{\partial \zeta}{\partial x} + v\frac{\partial \zeta}{\partial y} = w \qquad z = \zeta \qquad (9)$$

$$\frac{\partial h}{\partial t} + u\frac{\partial h}{\partial x} + v\frac{\partial h}{\partial y} = -w \qquad z = -h \qquad (10)$$

Using Leibnitz's Rule with conditions (9) and (10) and relations of type (7), we vertically integrate equations (4) between the limits $z = -h$ and $z = \zeta$ to yield

$$\frac{\partial \zeta}{\partial t} + \frac{\partial}{\partial x} \int_{-h}^{\zeta} u\,dz + \frac{\partial}{\partial y} \int_{-h}^{\zeta} v\,dz = 0$$

$$\frac{\partial}{\partial t} \int_{-h}^{\zeta} u\,dz + \frac{\partial}{\partial x} \int_{-h}^{\zeta} u^2\,dz + \frac{\partial}{\partial y} \int_{-h}^{\zeta} uv\,dz - f\int_{-h}^{\zeta} v\,dz = -\frac{\sigma^2}{k^2}\frac{\partial \zeta}{\partial x} + \frac{\tau_x^s - \tau_x^b}{\rho}$$

$$\frac{\partial}{\partial t} \int_{-h}^{\zeta} v\,dz + \frac{\partial}{\partial x} \int_{-h}^{\zeta} vu\,dz + \frac{\partial}{\partial y} \int_{-h}^{\zeta} v^2\,dz + f\int_{-h}^{\zeta} u\,dz = -\frac{\sigma^2}{k^2}\frac{\partial \zeta}{\partial y} + \frac{\tau_y^s - \tau_y^b}{\rho}$$

$$(11)$$

$\tau_x^s$ and $\tau_x^b$ are the x-components of the surface and bottom stresses, respectively. Similarly with the y-components.

We now follow Leendertse (1967) in writing

$$u = U(1 + \varepsilon_u)$$

$$v = V(1 + \varepsilon_v) \qquad (12)$$

where

$$U = \frac{1}{h + \zeta} \int_{-h}^{\zeta} u \, dz \, , \qquad V = \frac{1}{h + \zeta} \int_{-h}^{\zeta} v \, dz \qquad (13)$$

Thus $U(x, y)$ and $V(x, y)$ are the vertically averaged values of $u(x, y, z)$ and $v(x, y, z)$, respectively; and $\varepsilon_u(x, y, z)$ and $\varepsilon_v(x, y, z)$ express the fractional deviations of $u$ and $v$ from $U$ and $V$, respectively, at $x, y, z$.

Define the total height of the water column

$$H = h + \zeta$$

Then, using equations (12) and (13), the left hand sides of equations (11) become

$$\frac{\partial \zeta}{\partial t} + \frac{\partial HU}{\partial x} + \frac{\partial HV}{\partial y}$$

$$\frac{\partial HU}{\partial t} + \frac{\partial}{\partial x} \left\{ U^2 (H + \int_{-h}^{\zeta} \varepsilon_u^2 \, dz) \right\} + \frac{\partial}{\partial y} \left\{ UV(H + \int_{-h}^{\zeta} \varepsilon_u \, \varepsilon_v dz) \right\} - fHV$$

$$\frac{\partial HV}{\partial t} + \frac{\partial}{\partial x} \left\{ VU(H + \int_{-h}^{\zeta} \varepsilon_u \varepsilon_v dz) \right\} + \frac{\partial}{\partial y} \left\{ V^2 (H + \int_{-h}^{\zeta} \varepsilon_v^2 dz) \right\} + fHU$$

Assume isotropy of the horizontal velocity stratification. That is

$$\varepsilon_u(x, y, z) = \varepsilon_v(x, y, z) = \varepsilon(x, y, z) \qquad (14)$$

and let

$$H + \int_{-h}^{\zeta} \varepsilon^2 dz = \alpha H \qquad (15)$$

$\alpha(x, y, t)$ may be termed the "local velocity stratification factor" at time $t$. Always

$$\alpha \geq 1$$

With assumption (14) and definition (15), and after some reduction,

the equations governing the flow become

$$\frac{\partial \zeta}{\partial t} + \frac{\partial HU}{\partial x} + \frac{\partial HV}{\partial y} = 0$$

$$\frac{\partial U}{\partial t} + \alpha U \frac{\partial U}{\partial x} + \alpha V \frac{\partial U}{\partial y} - fV = -\frac{\sigma^2}{k^2 H} \frac{\partial \zeta}{\partial x} + \frac{\tau_x^s - \tau_x^b}{\rho H} - \{U^2 \frac{\partial \alpha}{\partial x} + UV \frac{\partial \alpha}{\partial y} + \frac{U}{H}(1 - \alpha \frac{\partial \zeta}{\partial t}\}$$

$$\frac{\partial V}{\partial t} + \alpha U \frac{\partial V}{\partial x} + \alpha V \frac{\partial V}{\partial y} + fU = -\frac{\sigma^2}{k^2 H} \frac{\partial \zeta}{\partial y} + \frac{\tau_y^s - \tau_y^b}{\rho H} - \{VU \frac{\partial \alpha}{\partial x} + V^2 \frac{\partial \alpha}{\partial y} + \frac{V}{H}(1 - \alpha)\frac{\partial \zeta}{\partial t}\}$$

(16)

If in equations (16) we put $\alpha = 1$ and replace $\sigma^2/k^2 H$ by g, we

obtain the Ha nsen long wave equations. From (6) we see that the second

replacement amounts to the equality

$$\tanh [kh] = kH$$

This will be closely approached for shallow water (or long) waves

provided $|\zeta| \ll h$.

## 3. Evaluation of the Velocity Stratification Factor

It is desired to evaluate $\alpha$ in closed form, using the results of

linear wave theory.

On the same level of approximation as equation (2)

$$u = \frac{gk}{\sigma} \frac{\cosh[k(h + z)]}{\cosh[kh]} \cdot \zeta \qquad -h \leq z \leq 0 \qquad (17)$$

From equations (3), (5) and (17) we have

$$\int_{-h}^{0} u dz = \frac{g\zeta}{\sigma}\tanh[kh]$$

Hence, approximately, by definition (13) and the last result

$$U = \frac{g\zeta \tanh[kh]}{\sigma H} \qquad (18)$$

and therefore, approximately

$$\zeta = \frac{U\sigma H}{g\tanh[kh]}$$

Substituting the last approximation for $\zeta$ in (17) yields

$$u = UkH \frac{\cosh[k(h + z)]}{\sinh[kh]}$$

whence, comparing with the first of equations (12)

$$1 + \epsilon = kH \frac{\cosh[k(h + z)]}{\sinh[kh]} \tag{19}$$

Now, by definition of $\epsilon$, we have

$$\int_{-h}^{\zeta} (1 + \epsilon)^2 \, dz = H + \int_{-h}^{\zeta} \epsilon^2 \, dz$$

Hence, from equations (15), (19), and the last result

$$\alpha H = \int_{-h}^{\zeta} k^2 H^2 \frac{\cosh^2[k(h + z)]}{\sinh^2[kh]} \, dz$$

from which

$$\alpha = \frac{1}{2} \frac{(kH)^2}{(\sinh[kh])^2} \left(1 + \frac{\sinh[2kH]}{2\,kH}\right)$$

It will be desirable, for computational reasons, that $\alpha$ should be a function of position only. To remove the time dependency of $\alpha$, we substitute h for H in the last result, and so obtain

$$\alpha = \frac{1}{2} \frac{(kh)^2}{(\sinh[kh])^2} \left(1 + \frac{\sinh[2kh]}{2\,kh}\right) \tag{20}$$

Equation (20) again only holds with the small amplitude assumption.

Some computed values of $\alpha$ between the asymptotic limits 1 and kh/2 are shown in Table 1.

<div align="center">

Table 1
Some Computed Values of $\alpha$

( See Tables Section of Report )

</div>

It appears that the Hansen equations are adequate well into the "intermediate wave" zone, and should yield fair accuracy for wavelengths as short as 3h.

## 4. The Two-Dimensional Numerical Model

Prior to the present study a two-dimensional, vertically-averaged, long wave computer model had been developed by McHugh (1976), utilizing

a mixed implicit-explicit method of solving the finite-difference equations derived from Leendertse (1967). The discretization was that shown in Figure 2.

**Fig. 2** Discretization of $\zeta$, h, U, V

A full account of the genesis of the model, which was designed to accomodate stretching of the grid lines and a time-varying land/water boundary, is given in McHugh (1976). The model was subsequently modified to allow randomly spaced grid lines, and this is the form utilized in the present work.

In order to generalize the long wave model to simulate waves of arbitrary length, it was merely necessary to insert into the momentum equations the factors $\alpha$ and the correction terms in braces as shown in equations (16); also to replace g in the pressure driving terms by $\sigma^2/k^2H = S^2/H$.

The bottom stress was represented through the Chézy coefficient, $C(x,y,t)$. Thus, $\tau_x^b = \dfrac{\rho g U (U^2 + V^2)^{1/2}}{C^2}$ , $\tau_y^b = \dfrac{\rho g V (U^2 + V^2)^{1/2}}{C^2}$

C values were computed from Manning's formula:
$$C = \frac{1.486 \; H^{1/6}}{n} \qquad (H \text{ in } ft.)$$

The resultant finite difference equations, which are very involved, have been presented as Appendix 1. Referring to this appendix, the superscript n (1, 2, 3...) denotes the time level $n\Delta t$. Barred quantities with subscript u or v denote two-point interpolated values at the

positions of U or V indicated. Quantities $V_{i,j}^*$ and $U_{i,j}^*$ denote four-point interpolations of V and U, respectively, centered at the locations of $U_{i,j}$ and $V_{i,j}$. All of these interpolations take into account the possible non-uniform grid spacing.

The quantities $I_i'$, $J_j'$ etc. are multipliers for determining derivatives when the grid spacing is irregular or stretched. In equation A(i) for instance, for irregular spacing:

$$I_{i+1/2}' = \frac{1}{x_{i+1} - x_i}$$

The notation derives from the form when $I = I(x)$ and $J = J(y)$ are stretching functions such that

$$\frac{\partial}{\partial x} = \frac{\partial}{\partial I}\frac{dI}{dx} \, , \, \frac{\partial}{\partial y} = \frac{\partial}{\partial J}\frac{dJ}{dy}$$

or, in finite difference operator form, writing I' for dI/dx and J' for dJ/dy

$$\frac{\Delta}{\Delta x} = \frac{\Delta}{\Delta I} I' \, , \, \frac{\Delta}{\Delta y} = \frac{\Delta}{\Delta J} J'$$

*Lower case subscripts have been used* in the equations for convenience.

Quantities $S_{i,j}$ and $\alpha_{i,j}$ were calculated at the centers of the corresponding grid squares. Two sorts of derivatives of $\alpha$ were used: those centered on the $\zeta$-points, and those centered on the U and V-points. The latter are distinguished by additional subscripts u or v in the manner already discussed. Thus for example

$$\alpha_{x i,j} = \frac{\alpha_{i+1,j} - \alpha_{i-1,j}}{1/2(x_{i+2} + x_{i+1} - x_1 - x_{i-1}}$$

$$\overline{\alpha}_{x u i,j} = \frac{\alpha_{i,j} - \alpha_{i-1,j}}{1/2(x_{i+1} - x_{i-1})}$$

with analogous expressions for $\alpha_{y i,j}$ and $\overline{\alpha}_{y v i,j}$.

For the constant boundary model, k(x, y), S (x, y), and $\alpha$(x, y) are calculated once and for all time over the entire wet field from equations (6), (8) and (20), respectively. Newton's iterative method

was found adequate for extracting k from equation (6). The first guess of k was the deep water value, $k_o$, given as input to the computer program. When the wet boundary changes with time (as for instance on a beach) there is the necessity of defining S and $\alpha$ in the newly flooded region. The strategy in the present study was to assume a default value $\alpha = 1$, and a default value $S^2/H = g$ in the initially dry regions ($h \leq 0$).

The implicit-explicit, double sweep solution technique has been described by Leendertse (1967) and McHugh (1976). Its principal stages are: (i) Solve implicitly for $\zeta^{n+1}$ and $U^{n+1}$ along each grid row. (ii) Solve explicitly for $V^{n+1}$ in each square of the wet field. (iii) Solve implicitly for $\zeta^{n+2}$ and $V^{n+2}$ along each grid column. (iv) Solve explicitly for $U^{n+2}$ in each square of the wet field. Repeat the procedure for the next pair of time steps, and so on. If the land/water boundary varies in time, this must be established periodically--eg., every two time steps--and allowance made for volume transport into previously dry areas (see Appendix 2).

A principle of the computation is to ignore derivatives when they cannot be computed from the central-difference formula owing to the proximity of a land boundary. This is found (Leendertse (1967)) to be beneficial for numerical stability.

Finally, the necessary boundary conditions required on a row or column are either the water level $\zeta$, or the input/output velocity U or V at all times. At a land boundary $U = V = 0$.

At the start of the model it is customary to assume $\zeta = 0$, and $U = V = 0$

everywhere inside the wet field.

## 5. Preliminary Tests of the Model

A 5 x 121 grid was selected initially with step lengths $\Delta x = \Delta y = $ **16 ft** (4.88 m). Three sides were closed thus forming a channel with dimensions 64 x 1920 ft. (19.52 x 585.60 m). For this geometry it will be convenient to consider the x-axis as running parallel to the longer dimension. Thus U is the onshore velocity component. For all tests with the channel a standard sinusoidal disturbance of water level was input at the open boundary having period 8 seconds and amplitude 1 ft. (0.305 m). The deep water wavelength $L_o$, deduced from equation (6) with tanh [kh] = 1, is then approximately 320 ft (97.60 m). With this $L_o$ the 16 ft. grid line separation yields 20 grid intervals per wavelength in deep water. If the bottom rises the wavelength will diminish, and it may be desirable to increase the grid resolution along x in the shallow region. Various resolution schemes were considered, maintaining however, a uniform grid interval along y of 16 ft.

Four depth contours were tested: (a) h constant at 150 ft. (45.75 m), (b) h varying linearly from 150 to 10 ft. (45.75 - 3.05 m), (c) varying linearly from 150 to - 3 ft. (45.75- -0.92 m), and (d) h varying linearly from 150 to - 3 ft. except in the region of a submerged bar. Contour (a) was used with both a closed (vertical wall) and open boundary "downstream". In (b) waves reflect off a vertical wall; in (c) and (d) waves reflect off a beach. Case (b), which is intermediate in effects between (a) and (c), may be called the "quasi-beach" config- uration; it was chosen to eliminate possible numerical distrubances arising from the changing land/water boundary, while preserving the effect of shoaling.

As earlier stated, in any wave computation equations (6) and (20) must be solved at all positive values of h for k and $\alpha$. Using equation (8) and the definition $L = 2\pi/k$, the wavelength L and phase speed S may be obtained for every grid square. Table 2 lists some values of L, S, and $\alpha$ for h-values within the range of the tests.

Table 2
Some values of L, S and $\alpha$ as Functions of h

## A.  Constant h: Deep Water Configuration

With h = 150 ft. it may be deduced from Table 2 that the wave should traverse the length of the channel in approximately 47 seconds. The computation was therefore allowed to simulate 52 seconds, with tabular output of $\zeta$, U, and V every 0.5 seconds. A time step was initially selected of 0.05 seconds. This is well below the Friedrichs-Lewy-Courant stability limit of 0.167 seconds for the considered grid interval and depth. Results for $\zeta$ and U with $\Delta t = 0.025$ seconds agreed in two places of decimals, hence we are close to solution convergence. The appropriate roughness coefficient for short waves over a 150 ft.-deep mud bottom being unknown, the value n = 0.026 was arbitrarily chosen. This value is typical of tidal models.

Fig. 3 Wave Profile for Deep Water Configuration (h=150ft.)
$\Delta$x=16ft., $\Delta$t=0.05sec., n=0.026

In Figure 3, which shows the wave profile at 48 seconds ($\zeta(i, 2)$, i=1,..120) it can be seen that the solution is numerically well behaved. The solution at 72 seconds (not shown) was also smooth and noise-free.

Figure 4 shows U plotted as a function of t for the grid point (80, 2). This point was chosen for examination as being in a region where the equilibrium wave profile was beginning to be established, yet not so close to the solid boundary as to invite interference from reflection effects.

Fig. 4 U as a Function of t for the Deep Water
Configuration at i-point 80
Note: 1ft/sec = 0.305m/sec.

According to equation (18) we may write approximately for deep water

$$U(z,t) = \frac{g\zeta}{\sigma h}$$

Since linear theory requires $\zeta$ to have the form

$$\zeta = a \sin(kx - \sigma t)$$

we have for the amplitude of U, with a =1 ft and $\sigma = 2\pi/8$ rad/sec

$$U' = \frac{ag}{\sigma h} = 0.273 \text{ ft/sec.}$$

The maxima and minima of Figure 4 are 0.283, -0.270, 0.294, -0.262, 0.290 ft /sec with mean absolute value 0.280 ft /sec. The difference from U' calculated above is less than 2%. Since the maxima and minima appear to be decreasing in absolute value the agreement would probably have been even better for a longer channel.

A second quantitative comparison between the model and theory is afforded by the so-called Stokes drift velocity, u*, integrated over the depth. Kinsman (1965) derives u* from the velocity potential in the form

$$u* = a^2k^2 \, Se^{2kz}$$

whence

$$\overline{u*} = \frac{a^2k^2S}{h} \int_{-h}^{0} e^{2kz} \, dz = \frac{a^2kS}{2h}$$

With $S = \sigma/k$ we have

$$\overline{U*} = \frac{a^2\sigma}{2h} = 0.00262 \text{ ft/sec.}$$

From the tabulated output of U at i-point 80 we estimate numerically

$$\overline{U} = \int_{0}^{T} \frac{U(h + \zeta)dt}{hT} \simeq \frac{\Sigma_j \, U_j \, H_j \, \Delta t'}{h \, \Sigma_j \, \Delta t'}$$

where T is the period, $U_j$, $H_j$ are tabulated values of U and H at time $t_j$, and $\Delta t'$ is the constant time interval (0.5 seconds). The j-summation is taken over a number of complete cycles of U. With the time limits for integration t = 28.5 seconds (U = 0.000 ft./sec) and t = 47.0 seconds (U = -0.010 ft /sec ), we have $\Sigma_j U_j H_j$ = 14.251 ft.$^2$/sec., $\Sigma_j \Delta t'$ = 18.5 seconds, and

$$\overline{U} = 0.00257 \text{ ft./sec}$$

The difference between $\overline{U}$ and $\overline{u*}$ is less than 2%.

## B. Linearly Varying h: Quasi-Beach Configuration

Figure 5 shows wave profiles at 60 and 61 seconds for a high resolution grid having $\Delta x$ = 16 ft for the first 90 intervals; $\Delta x$ = 8 ft. for the next 20 intervals; $\Delta x$ = 4 ft for the next 40 intervals; and $\Delta x$ = 2 ft. (0.61 m) for the last 80 intervals. The total length of the

grid is the same as in subsection A.

Fig. 5 Quasi-Beach Wave Profiles at 60 and 61 Seconds.
$\Delta x = 16$, 8, 4, 2ft , $\Delta t = 0.0125$sec., n=0.026

One sees clearly a breaking wave approaching the end wall.

In Figures 6a and 6b the time has been increased to 72 seconds. The higher resolution grid has $\Delta x = 16$ ft  for the first 90 intervals; $\Delta x = 8$ ft. for the next 20 intervals; and $\Delta x = 4$ ft. for the last 80 intervals, keeping the total length the same as in subsection A.

Fig. 6 Quasi-Beach Wave Profiles at 72 seconds; $\Delta t = 0.0125$ sec , n = 0.026 (a)  $\Delta x = 16$ ft , (b)  $\Delta x = 16$, 8, 4 ft.

Reflection of the breaking wave at the wall has apparently generated numerical noise propagating back into the channel. This noise exhibits wavelengths equal to simple multiples of the local grid spacing. As grid resolution increases, more spurious waves are generated per unit length of the channel in the noise affected area; and certain amplitudes may increase so much as to cause numerical instability, which is evidenced by fluctuating non-zero V-components in the transverse direction, and transverse oscillations of $\zeta$.

## Elimination of Grid-Induced Noise by Artificial Smoothing

An approach to the elimination of noise which has been found useful by tidal modelers is the so-called "artificial viscosity" strategy. One replaces certain dependent variables $X_{i,j}^n$ in the finite difference equations evaluated at the old time level n, with quantities $[X_{i,j}^n]$ defined, for a uniform grid, by

$$[X_{i,j}^n] = \beta X_{i,j} + 1/4(1 - \beta) \ (X_{i+1,j}^n + X_{i-1,j}^n + X_{i,j+1}^n + X_{i,j-1}^n)$$

$\beta$ is a dimensionless number with value usually between 0.99 and 1.0. A value of $\beta$ less than unity has the effect of lowering peaks and raising troughs relative to the mean of the variable $X_{i,j}^n$, hence smoothing it. In the finite difference equations of Appendix 1, artificially smoothed variables are enclosed by brackets [ ].

Some smoothing, and therefore de-energizing of the physically real wave will also result from this ploy; but it must be borne in mind that real world waves possess internal friction which the model represented by equations (16) does not. Hence one may be able to live with a slight smoothing of the longer wavelengths.

The 16-8-4 grid scheme was used with low bottom friction (n = 0.026) to test the effect of introducing $\beta < 1$ into the finite-difference equations. Figure 7 shows wave profiles at 72 and 73 seconds for a number of values of $\beta$. The uppermost trace corresponds to Figure 6b.

Fig. 7 Quasi-Beach Wave Profiles at 72 and 73 Seconds With Artificial Smoothing. $\Delta x$=16, 8, 4ft , $\Delta t$=0.0125sec , n=0.026

Almost identical traces to those for β = 0.995, Δt = 0.0125 sec ,
were obtained with β = 0.990, and Δt = 0.025 sec , showing that for
β < 1 the solutions become more sensitive to the time step than with
β = 1.  One thus has two degrees of parametric freedom, β and Δt, to
achieve the same degree of smoothing.

In the last pair of traces in Figure 7 the wave breaking effect
appears to have been virtually eliminated.  This may be useful for some
applications.

Another way of reducing the energy of numerical turbulence is to
introduce substantial bottom friction in the zone of wave breaking.

Figure 8 shows wave profiles at 72 and 73 seconds for the highest
resolution grid (16-8-4-2) and a Manning's n distributed as in the
figure caption.  The width of the zone with n = 5 is approximately 54
ft  (16.5 m).  The unsmoothed profiles (β = 1) have been given for
comparison with smoothed profiles, β = 0.997.

Fig. 8 Quasi-Beach Wave Profiles at 72 and 73 Seconds With Combined
High Bottom Friction and Artificial Smoothing.
Δx = 16,8,4,2 ft , Δt = 0.025 sec , n = 0.026, h ≥ 20 ft.; n =
0.2, 14 ft ≤ h < 20 ft ; n = 5, h < 14 ft.

## C.  Linearly Varying h: Beach Configuration

This configuration involves a time-varying land/water boundary.
For a brief description of the handling of this problem see Appendix 2.

Figure 9 shows the wave profile at 76 seconds for the uniform
coarse grid and the lowest bottom friction without numerical smoothing.

Grid-generated noise is present near the shoreline. Increasing the resolution of the grid for this low bottom friction resulted in unstable solutions for all grid schemes considered.

Fig. 9 Beach Wave Profile at 76 Seconds
$\Delta x$ = 16 ft , $\Delta t$ = 0.0125 sec , n = 0.026

Using the 16-8-4 grid scheme and n = 0.026, all values of $\beta$ down to 0.99 did not succeed in removing the transverse numerical instability at 76 seconds. At $\beta$ = 0.95, the wave height in the zone x > 1440 ft. was less than 0.2 ft (0.06 m); hence n = 0.026 is not a viable Manning coefficient for the beach configuration even with artificial energy loss.

In Figure 10 we have wave profiles at 76 seconds for the 16-8-4 grid scheme and a Manning's n distribution as given in the caption. The slight noise in the unsmoothed trace has been almost eliminated in the trace with $\beta$ = 0.997.

Fig. 10 Beach Wave Profiles at 76 Seconds
$\Delta x$ = 16,8,4, $\Delta t$ = 0.025 sec , n = 0.026, h $\geq$ 20 ft ; n = 0.2, 10 ft $\leq$ h < 20 ft ; n 0.5, h < 10 ft.

## D. Linearly Varying h—Beach Plus Offshore Bar

Figure 11 shows the wave profile at 60 seconds that was obtained for the bar geometry shown inset, using the uniform coarse grid. The bar ridge, 48 ft  (14.6 m) wide is approximately 6 ft  (1.83 m) deep and 368 ft  (112.2 m) offshore.

Fig. 11 Beach-With-Bar Wave Profile at 60 Seconds
$\Delta x = 16$ ft , $\Delta t$  0.05 sec , n = 0.026

There is probably noise present in the wave trace, as suggested by the experience of Figure 9.  Significant results, however, could doubtless be obtained by a judicious choice of bottom friction over the bar, a better grid resolution in the same neighborhood, and some artificial smoothing.

## E. Constant h:  Deep Water Configuration With Open Boundary Downstream

If a beach or other kind of closed downstream boundary is not desired, an open boundary or reactionless gate to the passage of the waves may be simulated by an appropriate adjustment of either the water level in the last grid square, or the U-value on the boundary, at all times.

Let the maximum value of grid coordinate i be K, and let $(n+2)\Delta t$ be the new time level at which boundary values of $\zeta$ or U must be given. We write

$$\zeta^{n+2}_{K-1,j} = \zeta^{n+1}_{K-1,j} - \frac{(\zeta^{n+1}_{K-1,j} - \zeta^{n+1}_{K-2,j})}{\Delta x_{K-1}} S_{K-1,j} \Delta t \tag{i}$$

$$U^{n+2}_{K,j} = U^{n+1}_{K,j} - \frac{(U^{n+1}_{K,j} - U^{n+1}_{K-1,j})}{\Delta x_{K-1}} S_{K-1,j} \Delta t \tag{ii}$$

Both schemes (i) and (ii) were tested and found to yield comparable results. The discussion will be confined to shceme (ii) where the boundary value of the velocity is extrapolated from the interior field value at the earlier time step.

Figure 12(a) shows the wave profile at 28 seconds that resulted when the input boundary $\zeta$ was set equal to zero for $t \geq 24$ seconds. A wave pocket has been caught in its parrage toward the right hand boundary. In Figure 12(b) at 72 seconds, the wave packet has vanished through the open right hand boundary simulated by means of equation (ii) above.

Fig. 12 Wave Profiles for Deep Water Configuration (h = 150 ft.)
With Open Downstream Boundary. $\zeta(1,j) = 0, t \geq 24$ sec.
$\Delta x = 16$ ft, $\Delta t = 0.025$ sec, n = 0.026, $\beta = 1$

## 6. Wide Area Grid—Breakwater Parallel to Beach

As a test of the ability of the model to predict longshore effects, a plane wave with parameters the same as those considered above, was allowed to travel past a breakwater extending half way across the 1904 x 1840 ft (580.7 x 561.2 m) grid selected, the bottom contour elsewhere corresponding to the beach configuration already described

(h = 150 to -3 ft.).  Grid dimensions were 120 x 116, with $\Delta x = \Delta y = 16$ ft  (4.9 m).  The vertically uniform breakwater, 16 ft  thick, was positioned in the row i = 93, where the water depth is 30.7 ft  (9.4 m), and extended 928 ft  (283 m) from the edge of the grid, parallel to y. It was thus about 360 ft. (110 m) offshore.  Lateral boundaries to the grid were closed.  A constant Manning coefficient of 0.026 was assumed. There was no artificial smoothing.

Figure 13 shows schematically the positions of the wave crests at t = 64 seconds.  It was obtained by printing symbolic depths, $h_s$, such that $\zeta > 0$, $h_s = 1$; $\zeta < 0$, $h_s = 0$, and linking the 0's by shading. Hence white areas correspond to water above z = 0, and shaded areas to water below this level.  Clearly, there is a diffraction of the wave fronts around the breakwater.  Substantial values of V occurred in the sheltered region, also on the seaward side of the breakwater.

Fig. 13 Wave Crests at 64 Seconds for the Beach-Breakwater Config-
uration
$\Delta x = \Delta y = 16$ ft , $\Delta t = 0.2$ sec , n = 0.026

## 7.  Conclusions

A model solving vertically integrated three-dimensional equations with borrowings from lineary wave theory, has been shown to account for short waves in deep water very well.  Problems due to numerical turbu-

lence are likely to arise, however, in shallow water where the small
amplitude approximation no longer holds, and—most significantly—wave
breaking leads to a multi-valued solution for the water level at a
point. This difficluty can be overcome if the shallow zone is treated
as a buffer of very high bottom friction, and some internal energy loss
(smoothing) is employed. In effect, a beach is replaced by a shock-
absorbent wall. Such an approach is likely to be satisfactory for
computations where offshore processes rather than beach processes are of
interest.

## 8. References

Giles, R. V., "Fluid Mechanics and Hydraulics," McGraw Hill, New York, 1962, pp. 135-136.

Hansen, W., "Theorie zur Errechrung des Wasserstandes und der Stromunger in Randmeerer nebst Anwedungen," Tellus, Vol. 8, No. 3, 1956, pp. 287-300.

Ippen, A. T., ed., Estuary and Coastline Hydrodynamics, McGraw-Hill, New York, 1966.

Kinsman, B., Wind Waves, Prentice-Hall, Inc., Englewood Cliffs, New Jersey, 1965, 676 p.

Leendertse, J. J., Aspects of a Computational Model for Long-Period Water Wave Propagation, Rand Corp., Memo. RM-5294-PR, 1967.

McHugh, G. F., Development of a Two-Dimensional Hydrodynamic Numerical Model for Use in a Shallow, Well-Mixed Estuary, Louisiana State University Center for Wetland Resources, Baton Rouge, La. Sea Grant Publ. No. LSU-T-76-008, 1976.

$$\frac{\zeta_{i,j}^{n+1} - [\zeta_{i,j}^{n}]}{\Delta t} + (\overline{Hu}_{i+1,j}^{n} \, U_{i+1,j}^{n+1} - \overline{Hu}_{i,j}^{n} \, U_{i,j}^{n+1}) \, \overline{I}_{i+1/2}'$$

$$+ (\overline{Hv}_{i,j+1}^{n} \, V_{i,j+1}^{n} - \overline{Hv}_{i,j}^{n} \, V_{i,j}^{n}) \, \overline{J}_{j+1/2}' \quad = 0 \qquad\qquad A(i)$$

$$\frac{U_{i,j}^{n+1} - [U_{i,j}^{n}]}{\Delta t} + \overline{\alpha}u_{i,j} \, U_{i,j}^{n+1} \, \frac{(U_{i+1,j}^{n} - U_{i-1,j}^{n})}{2} \, I_{i}' + \overline{\alpha}u_{i,j} \, V_{i,j}^{*n} \, \frac{(U_{i,j+1}^{n} - U_{i,j-1}^{n})}{2} \, \overline{J}_{j+1/2}'$$

$$- f \, V_{i,j}^{*n} + \frac{\overline{Su}_{i,j}^{2}}{2\overline{Hu}_{i,j}^{n}} \, [(\zeta_{i,j}^{n+1} - \zeta_{i-1,j}^{n+1}) + (\zeta_{i,j}^{n} - \zeta_{i-1,j}^{n})] \, I_{i}'$$

$$+ \frac{g}{2} (U_{i,j}^{n+1} + [U_{i,j}^{n}]) \, [[U_{i,j}^{n}]^{2} + (V_{i,j}^{*n})^{2}]^{1/2} / \overline{Hu}_{i,j}^{n} \, (\overline{Cu}_{i,j}^{n})^{2} - \tau_{x}^{s} / \rho\overline{Hu}_{i,j}^{n} \qquad A(ii)$$

$$+ U_{i,j}^{n}[U_{i,j}^{n} \, \overline{\alpha}xu_{i,j} + V_{i,j}^{*n} \, \alpha y_{i,j} + (1-\overline{\alpha}u_{i,j}) \left(\frac{\partial\zeta}{\partial t}\right)^{n}/\overline{Hu}_{i,j}^{n}] = 0$$

$$\frac{V_{i,j}^{n+1} - [V_{i,j}^n]}{\Delta t} + \overline{\alpha v}_{i,j} \; U_{i,j}^{*n+1} \frac{(V_{i+1,j}^n - V_{i-1,j}^n)}{2} \; \overline{I}'_{i+1/2} + \overline{\alpha v}_{i,j} \; V_{i,j}^{n+1} \frac{(V_{i,j+1}^n - V_{i,j-1}^n)}{2} J'_j$$

$$+ f \; U_{i,j}^{*n+1} + \frac{\overline{S v}_{i,j}^2}{2\overline{H v}_{i,j}^{n+1}} \; [(\zeta_{i,j}^{n+1} - \zeta_{i,j-1}^{n+1}) + (\zeta_{i,j}^n - \zeta_{i,j-1}^n)] \; J'_j \qquad\qquad \text{A(iii)}$$

$$+ g \; V_{i,j}^{n+1} \; [(U_{i,j}^{*n+1})^2 + [V_{i,j}^n]^2]^{1/2} / \overline{H v}_{i,j}^{n+1} \; (\overline{C v}_{i,j}^{n+1})^2 - \tau_y^s / \rho \; \overline{H v}_{i,j}^{n+1}$$

$$+ V_{i,j}^n \; [U_{i,j}^{*n+1} \alpha x_{i,j} + V_{i,j}^n \; \overline{\alpha y v}_{i,j} + (1 - \overline{\alpha v}_{i,j})\left(\frac{\partial \zeta}{\partial t}\right)^n / \overline{H v}_{i,j}^{n+1}] = 0$$

$$\frac{\zeta_{i,j}^{n+2} - [\zeta_{i,j}^{n+1}]}{\Delta t} + (\overline{H u}_{i+1,j}^{n+1} \; U_{i+1,j}^{n+1} - \overline{H u}_{i,j}^{n+1} \; U_{i,j}^{n+1}) \quad \overline{I}'_{i+1/2}$$

$$\qquad\qquad\qquad\qquad\qquad\qquad\qquad\qquad\qquad\qquad\qquad\qquad \text{A(iv)}$$

$$+ (\overline{H v}_{i,j+1}^{n+1} \; V_{i,j+1}^{n+2} - \overline{H v}_{i,j}^{n+1} \; V_{i,j}^{n+2}) \quad \overline{J}'_{j+1/2} \quad = \quad 0$$

$$\frac{V_{i,j}^{n+2} - [V_{i,j}^{n+1}]}{\Delta t} + \overline{\alpha v}_{i,j} \; U_{i,j}^{*n+1}\frac{(V_{i+1,j}^{n+1} - V_{i-1,j}^{n+1})}{2} \; \overline{I}'_{i+1/2} + \overline{\alpha v}_{i,j} \; V_{i,j}^{n+2} \frac{(V_{i,j+1}^{n+1} - V_{i,j-1}^{n+1})}{2} J'_j$$

$$+ f \; U_{i,j}^{*n+1} + \frac{\overline{S v}_{i,j}^2}{2\overline{H v}_{i,j}^{n+1}} \; [(\zeta_{i,j}^{n+2} - \zeta_{i,j-1}^{n+2}) + (\zeta_{i,j}^{n+1} - \zeta_{i,j-1}^{n+1})] \; J'_j$$

$$+ \frac{g}{2} (V_{i,j}^{n+2} + [V_{i,j}^{n+1}]) \; [(U_{i,j}^{*n+1})^2 + [V_{i,j}^{n+1}]^2]^{1/2} / \overline{H v}_{i,j}^{n+1} \; (\overline{C v}_{i,j}^{n+1})^2 - \tau_y^s / \rho \overline{H v}_{i,j}^{n+1} \qquad \text{A(v)}$$

$$+ V_{i,j}^{n+1} \; [U_{i,j}^{*n+1} \; \alpha x_{i,j} + V_{i,j}^{n+1} \; \overline{\alpha y v}_{i,j} + (1 - \overline{\alpha v}_{i,j})\left(\frac{\partial \zeta}{\partial t}\right)^{n+1} / \overline{H v}_{i,j}^{n+1}] = 0$$

$$\frac{U^{n+2}_{i,j} - [U^{n+1}_{i,j}]}{\Delta t} + \overline{\alpha}u_{i,j}\, U^{n+2}_{i,j}\, \frac{(U^{n+1}_{i+1,j} - U^{n+1}_{i-1,j})}{2}\, I'_i\, + \overline{\alpha}u_{i,j}\, V^{*n+2}_{i,j}\, \frac{(U^{n+1}_{i,j+1} - U^{n+1}_{i,j-1})}{2}\, \overline{J}'_{j+1/}$$

$$- f\, V^{*n+2}_{i,j} + \frac{\overline{5}u^2_{i,j}}{2\overline{H}u^{n+2}_{i,j}}\, [(\zeta^{n+2}_{i,j} - \zeta^{n+2}_{i-1,j}) + (\zeta^{n+1}_{i,j} - \zeta^{n+1}_{i-1,j})]\quad I'_i$$

$$+ g\, U^{n+2}_{i,j}\, [[U^{n+1}_{i,j}]^2 + (V^{n+2}_{*i,j})^2]^{1/2}\, /\overline{H}u^{n+2}_{i,j}\, (\overline{C}u^{n+2}_{i,j})^2\ -\ \tau^s_x/\, \rho\, \overline{H}u^{n+2}_{i,j} \qquad A(vi)$$

$$+ U^{n+1}_{i,j}\, [U^{n+1}_{i,j}\, \overline{\alpha}xu_{i,j} + V^{*n}_{i,j}\, \alpha y_{i,j} + (1 - \overline{\alpha}u_{i,j})\, \left(\frac{\partial\zeta}{\partial t}\right)^{n+1}/\overline{H}u^{n+2}_{i,j}]\ =\ 0$$

$$A(ii):\quad \left(\frac{\partial\zeta}{\partial t}\right)^n = -(\overline{HU}^n_{i+1,j}U^n_{i+1,j} - \overline{HU}^n_{i,j}\, U^n_{i,j})\overline{I}'_{i+1/2} - (\overline{HV}^n_{i,j+1}\, V^n_{i,j+1} - \overline{HV}^n_{i,j}\, Vn_{i,j})\overline{J}'_{j+1/2}$$

$$A(iii):\quad \left(\frac{\partial\zeta}{\partial t}\right)^n = -(\overline{H}u^{n+1}_{i+1,j}\, U^{n+1}_{i+1,j} - \overline{H}u^{n+1}_{i,j}\, U^{n+1}_{i,j})\overline{I}'_{i+1/2} - (\overline{H}v^{n+1}_{i,j+1}\, V^n_{i,j+1} - \overline{H}v^{n+1}_{i,j}\, V^n_{i,j})\overline{J}'_{j+1/2}$$

$$A(V):\quad \left(\frac{\partial\zeta}{\partial t}\right)^{n+1} = -(\overline{H}u^{n+1}_{i+1,j}\, U^{n+1}_{i+1,j} \cdot \overline{H}u^{n+1}_{i,j}\, U^{n+1}_{i,j})\overline{I}'_{i+1/2} - (\overline{H}v^{n+1}_{i,j+1}\, V^{n+1}_{i,j+1} - \overline{H}v^{n+1}_{i,j}\, V^{n+1}_{i,j})\overline{J}'_{j+1/2}$$

$$A(V1):\quad \left(\frac{\partial\zeta}{\partial t}\right)^{n+1} = -(\overline{H}u^{n+2}_{i+1,j}\, U^{n+1}_{i+1,j} - \overline{H}u^{n+2}_{i,j}\, U^{n+1}_{i,j})\overline{I}'_{i+1/2} - (\overline{H}v^{n+2}_{i,j+1}\, V^{n+2}_{i,j+1} - \overline{H}v^{n+2}_{i,j}\, V^{n+2}_{i,j})\overline{J}'_{j+1/2}$$

## Appendix 2 - Note on the Treatment of the Varying Land/Water Boundary

The time-varying land/water boundary for the beach model was handled by a method described in McHugh (1976). Immediately following the second, fourth, sixth, etc., time steps, a call is made to a program subroutine that determines whether flooding of a dry square can occur, and if so, transfers water into the dry square. The criterion for flooding is, in the case of a one-dimensional bottom slope parallel to

x:    $\zeta_{i-1} > -h_{i,j}$

The transferred water volume $\Delta v$ is calculated from the formula

$$\Delta v = 0.52b \ (\zeta_{i-1,j} + h_{i,j})^{3/2} \ \Delta t$$

where $b = 3.33$ is the Francis weir constant ( Giles (1962)). This formula is obtained by time integration of a variable crest weir flow over the interval $2\Delta t$, assuming the water level in the flooding square exceeds the bottom level in the flooded square during all of $2\Delta t$. The argument for this assumption in the case of the beach model is as follows: First, define a critical depth $H_c$ below which a newly flooded square is considered still "dry". This strategy was adopted to avoid certain numerical problems (McHugh 1976). In the present study $H_c = 0.1$ ft. (0.03 m). With wave period 8 seconds and amplitude 1 ft. the water only rises approximately 0.01 ft. in 0.02 seconds, so that the new depth established in a dry square after flooding during time $2\Delta t = 0.025$ seconds, say, will be very much less than $H_c$. Consequently, several applications of the flooding formula will be necessary to establish a new depth greater than $H_c$. This means that for the second and all subsequent necessary applications $\zeta_{i-1,j}$ will already exceed $-h_{i,j}$ at the beginning of the interval $2\Delta t$.

The reverse situation to flooding of a grid square is ebbing of water from it. In general, when ebbing occurs a negative depth will be established by the computer program. This represents a volume debt to the wet field that must be restored by the program to conserve water volume ( McHugh 1976).

### Table 1

Some Computed Values of $\alpha$

|  | kh | $\alpha$ |
|---|---|---|
| Long Waves (Shallow water) | 0 | 1 |
|  | 0.3 | 1.00 |
| Intermediate Waves | 1 | 1.02 |
|  | 2 | 1.18 |
|  | 3 | 1.53 |
| Short Waves (Deep water) | $\infty$ | kh/2 |

### Table 2

Some Values of L, S and $\alpha$ as Functions of h

| h ft | L ft | S ft./sec. | $\alpha$ |
|---|---|---|---|
| 150.00 | 325.7 | 40.71 | 1.51 |
| 79.89 | 304.3 | 38.04 | 1.10 |
| 10.00 | 135.3 | 16.91 | 1.00 |
| 1.03 | 25.5 | 3.19 | 1.00 |
| 0.33 | 8.9 | 1.12 | 1.00 |

Note: 1 ft = 0.305 m
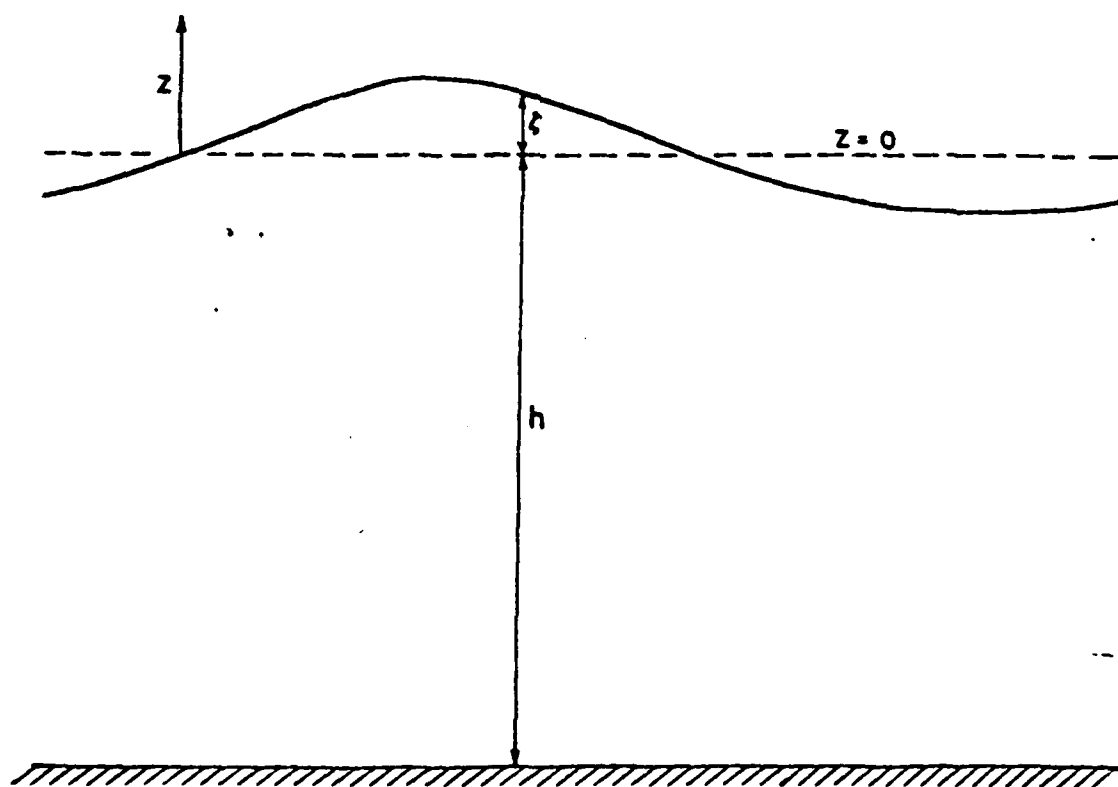
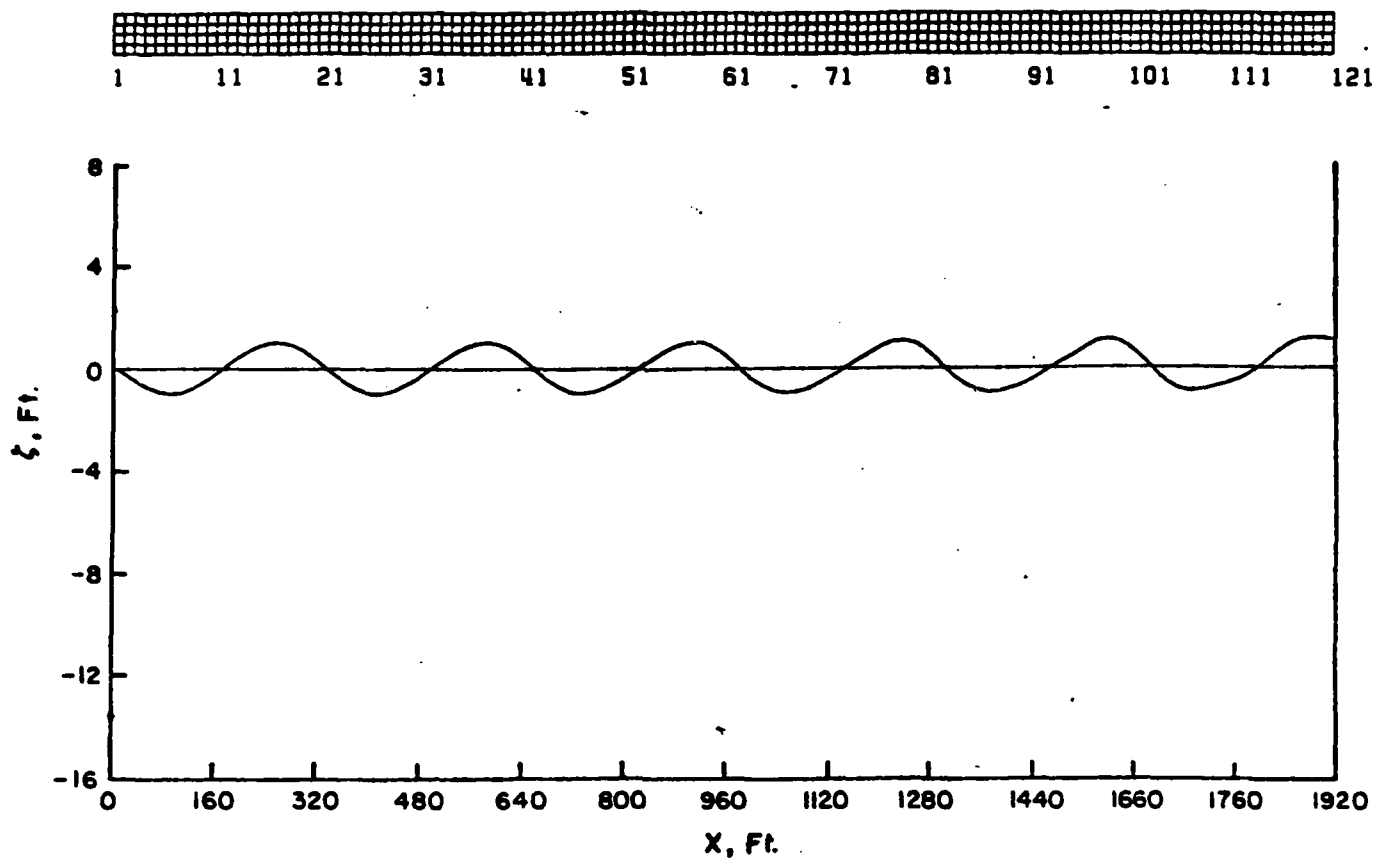Fig. 1 Definition Diagram of z, h. ζ
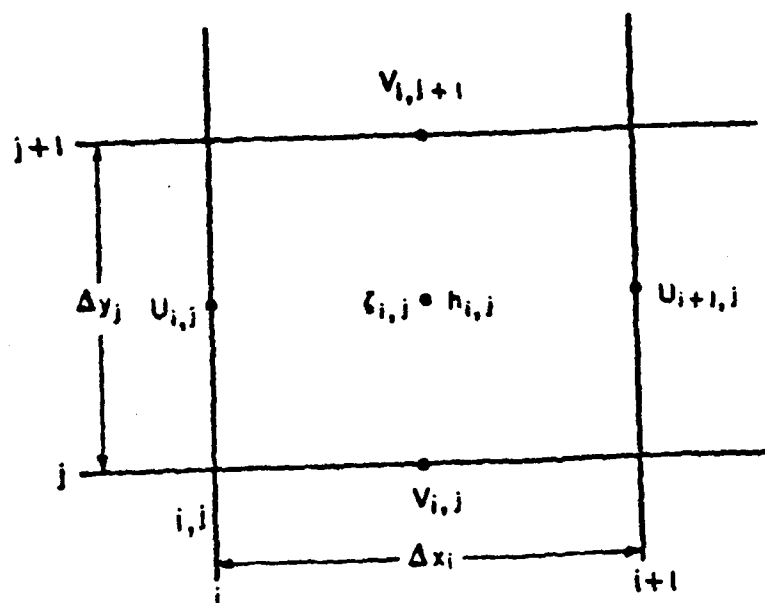
Fig. 2  Discretization of $\zeta$, h, U, V

Fig. 3 Wave Profile for Deep Water Configuration (h=150ft.)
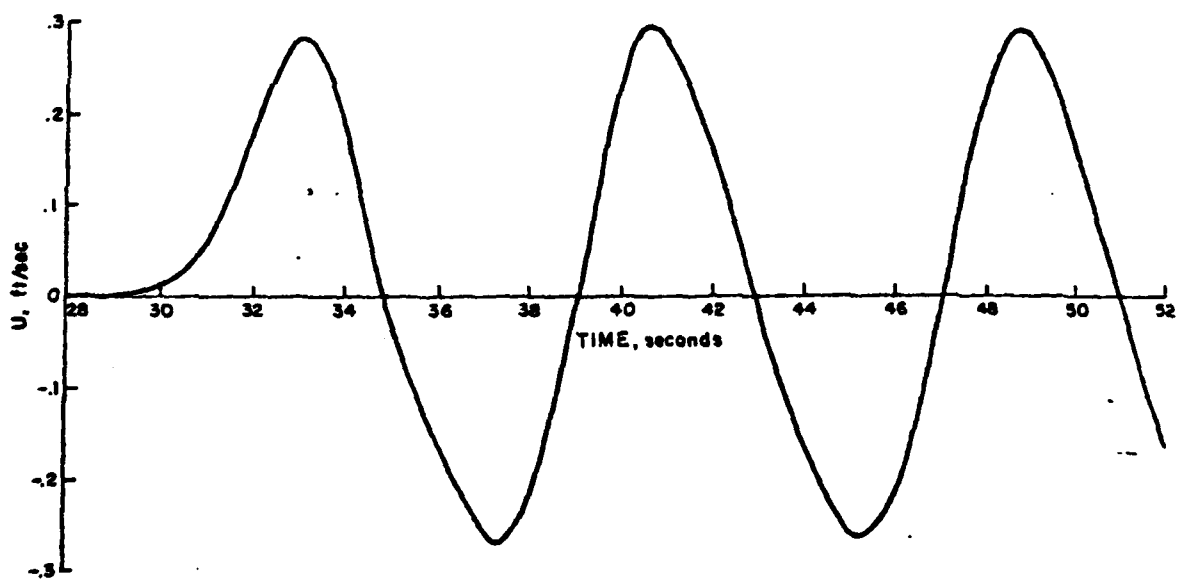$\Delta x = 16$ft., $\Delta t = 0.05$sec., $n = 0.026$

Fig. 4 U as a Function of t for the Deep Water
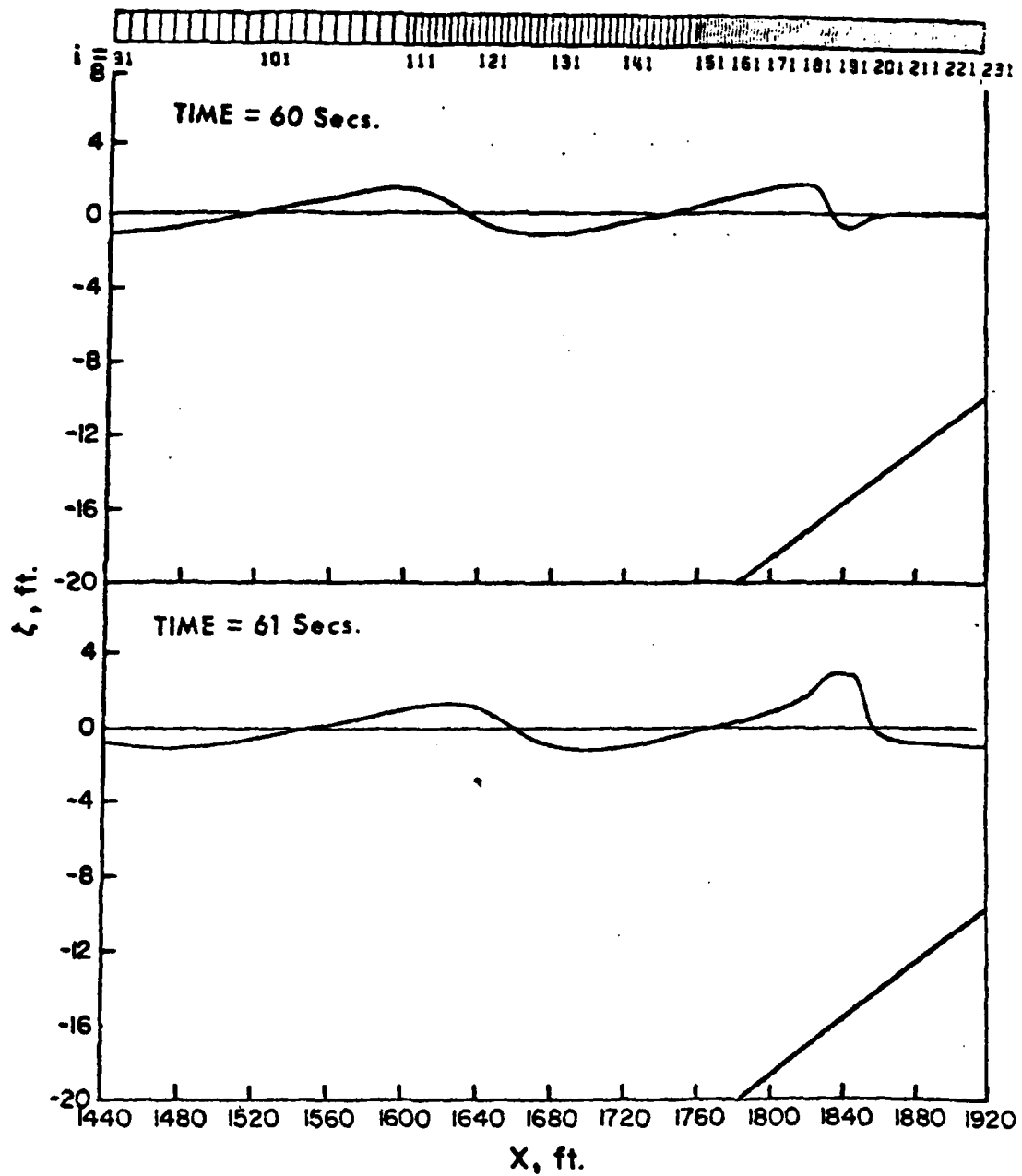Configuration at L-point 80
Note: 1ft/sec. = 0.305m/sec.

Fig. 5 Quasi-Beach Wave Profiles at 60 and 61 Seconds.
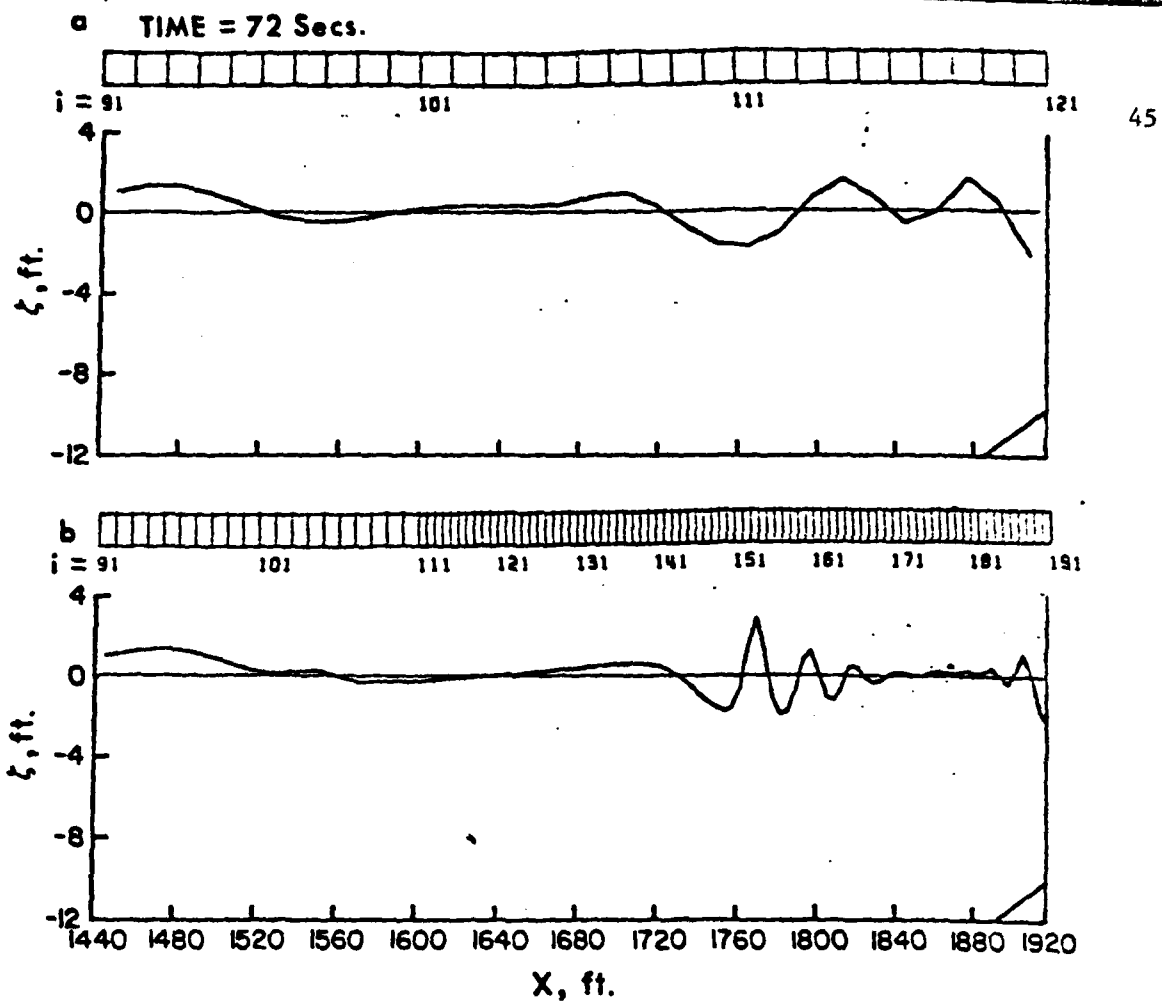$\Delta x$=16, 8, 4, 2ft., $\Delta t$=0.0125sec., n=0.026

**a**    TIME = 72 Secs.

Fig. 6 Quasi-Beach Wave Profiles at 72 seconds; $\Delta t$ = 0.0125 sec., n
= 0.026 (a) $\Delta x$ = 16 ft., (b) $\Delta x$ = 16, 8, 4 ft.
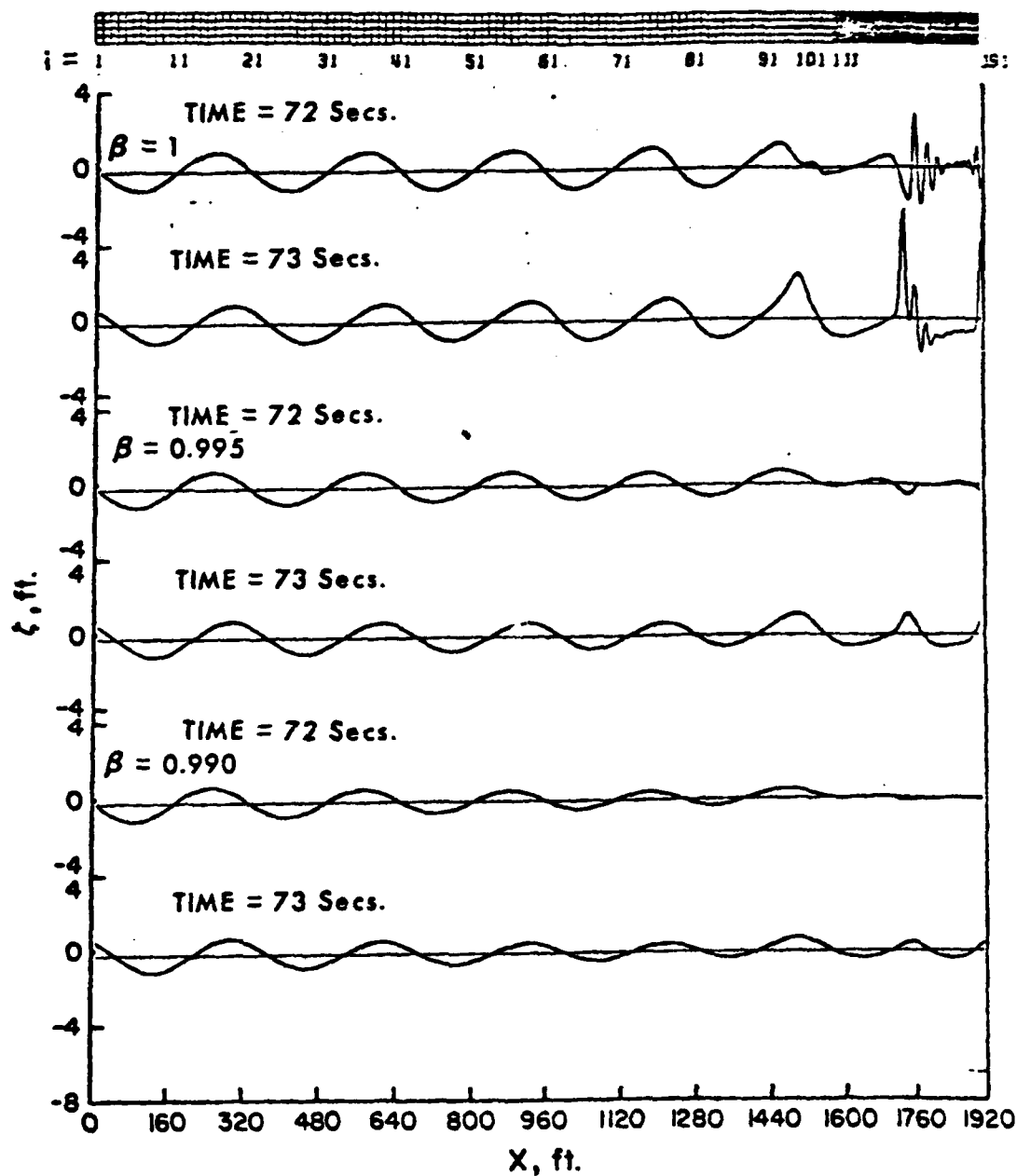
Fig. 7 Quasi-Beach Wave Profiles at 72 and 73 Seconds With Artificial
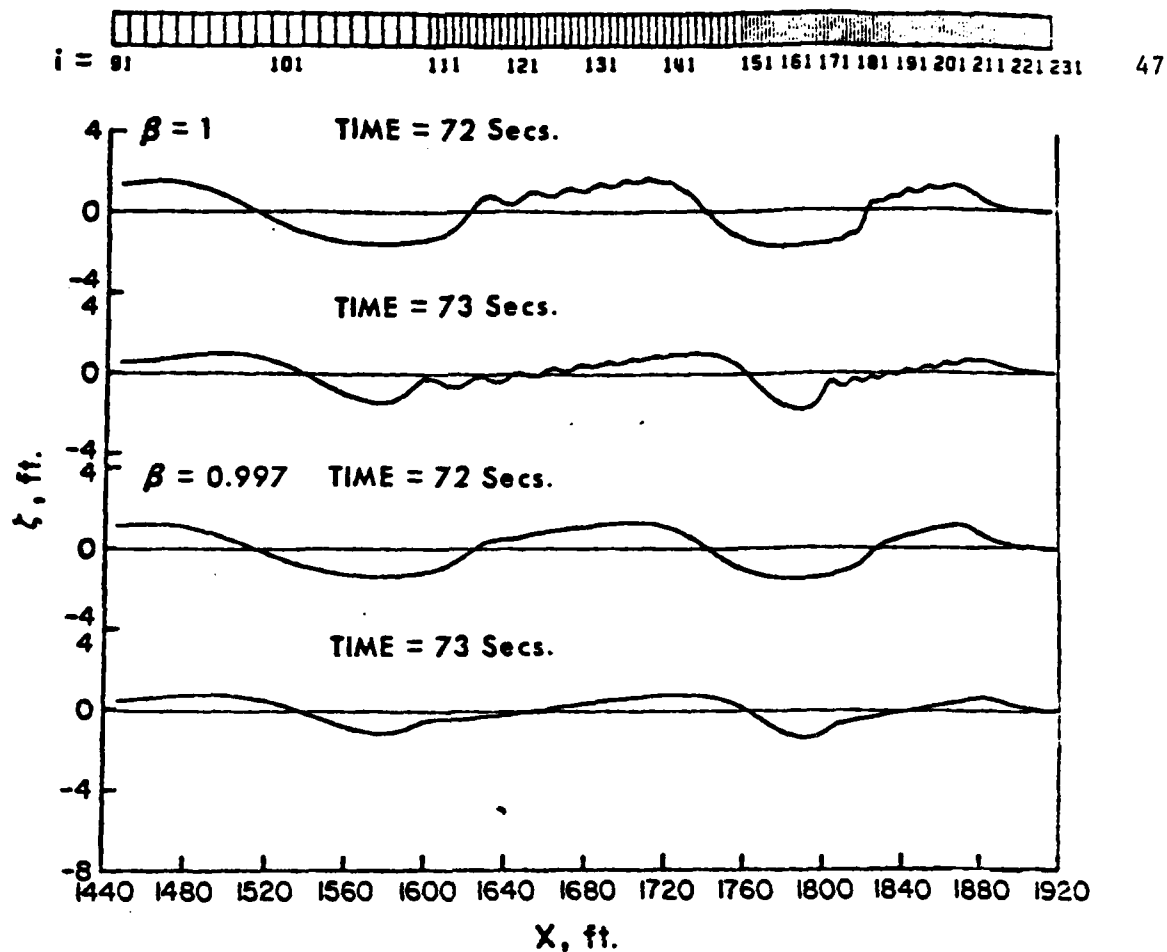Smoothing. Δx=16, 8, 4ft., Δt=0.0125sec., n=0.026

Fig. 8 Quasi-Beach Wave Profiles at 72 and 73 Seconds With Combined
High Bottom Friction and Artificial Smoothing.
$\Delta x = 16, 8, 4, 2$ ft., $\Delta t = 0.025$ sec., $n = 0.026$, $h \geq 20$ ft.; $n = 0.2$, $14$ ft. $\leq h < 20$ ft.; $n = 5$, $h < 14$ ft.

TIME = 76 Secs.
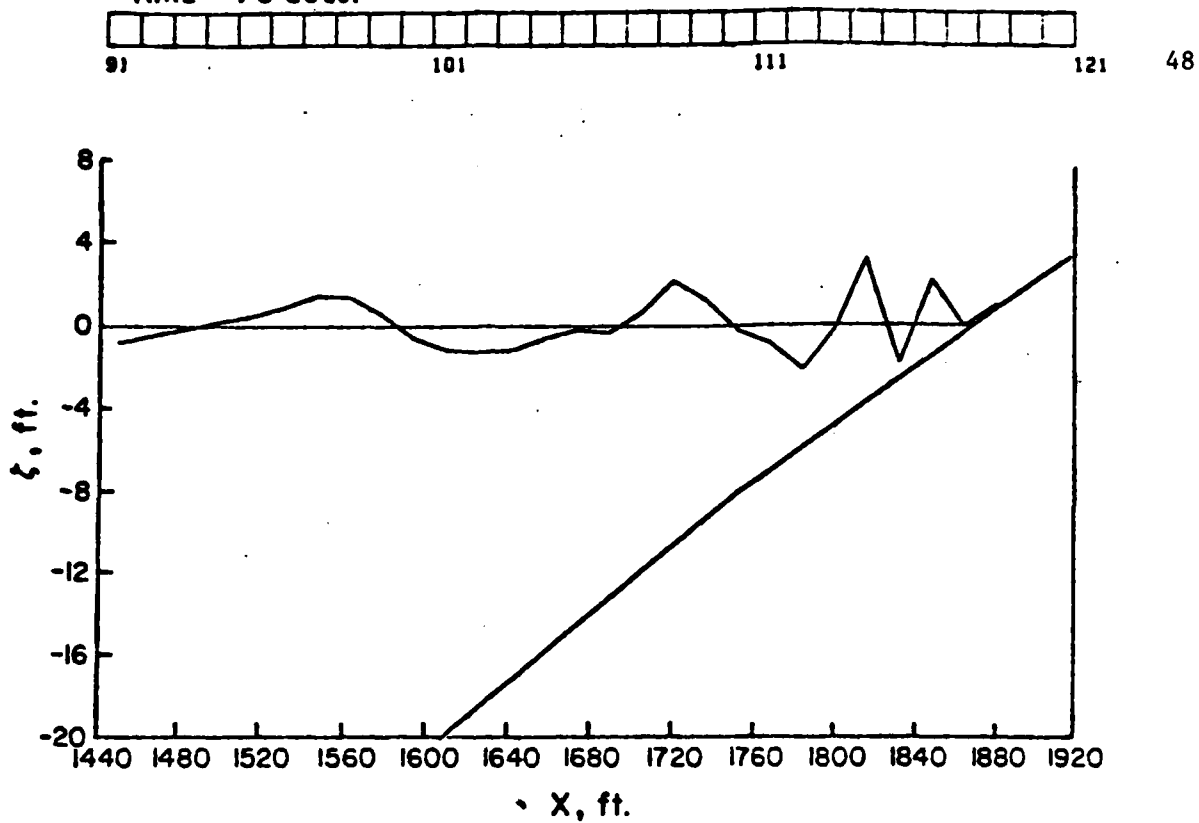


Fig. 9 Beach Wave Profile at 76 Seconds
$\Delta x = 16$ ft., $\Delta t = 0.0125$ sec., n = 0.026
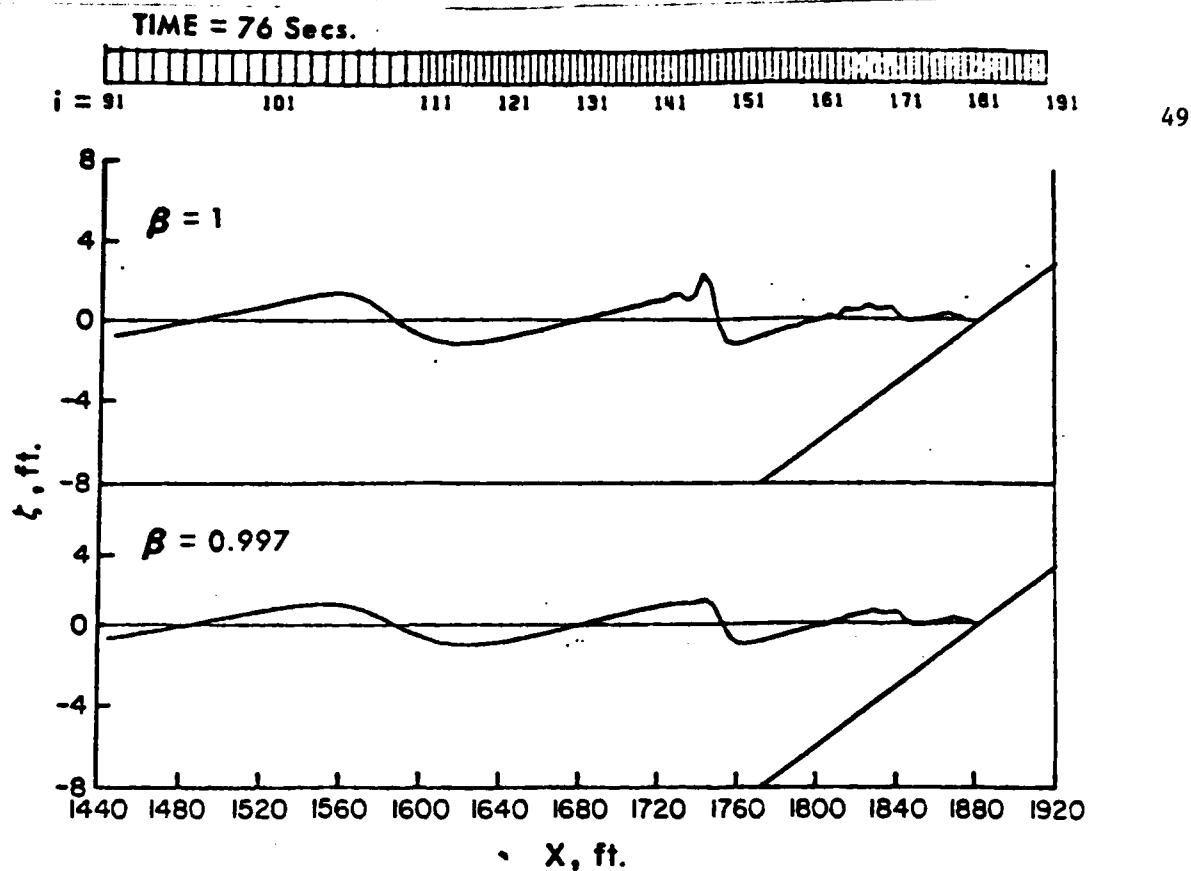
Fig. 10 Beach Wave Profiles at 76 Seconds
$\Delta x = 16,8,4$, $\Delta t = 0.025$ sec., n = 0.026, h > 20 ft.; n = 0.2, 10
ft. $\leq$ h < 20 ft.; n  0.5, h < 10 ft.
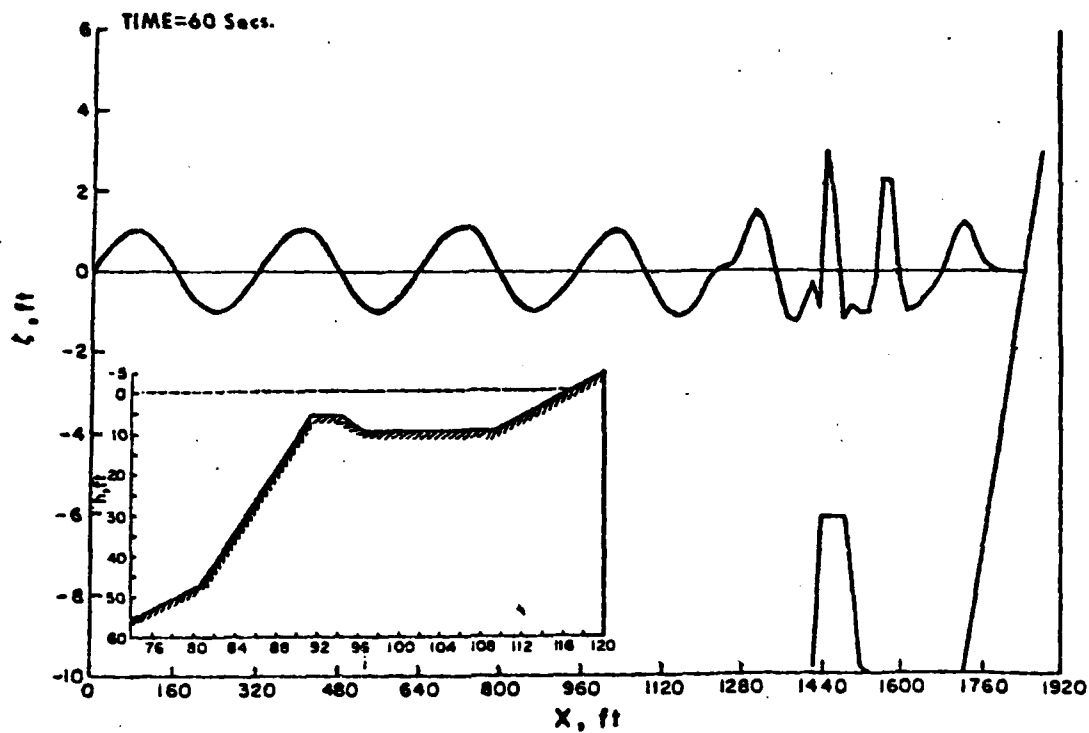
Fig. 11 Beach-With-Bar Wave Profile at 60 Seconds
$\Delta x = 16$ ft., $\Delta t = 0.05$ sec , $n = 0.026$
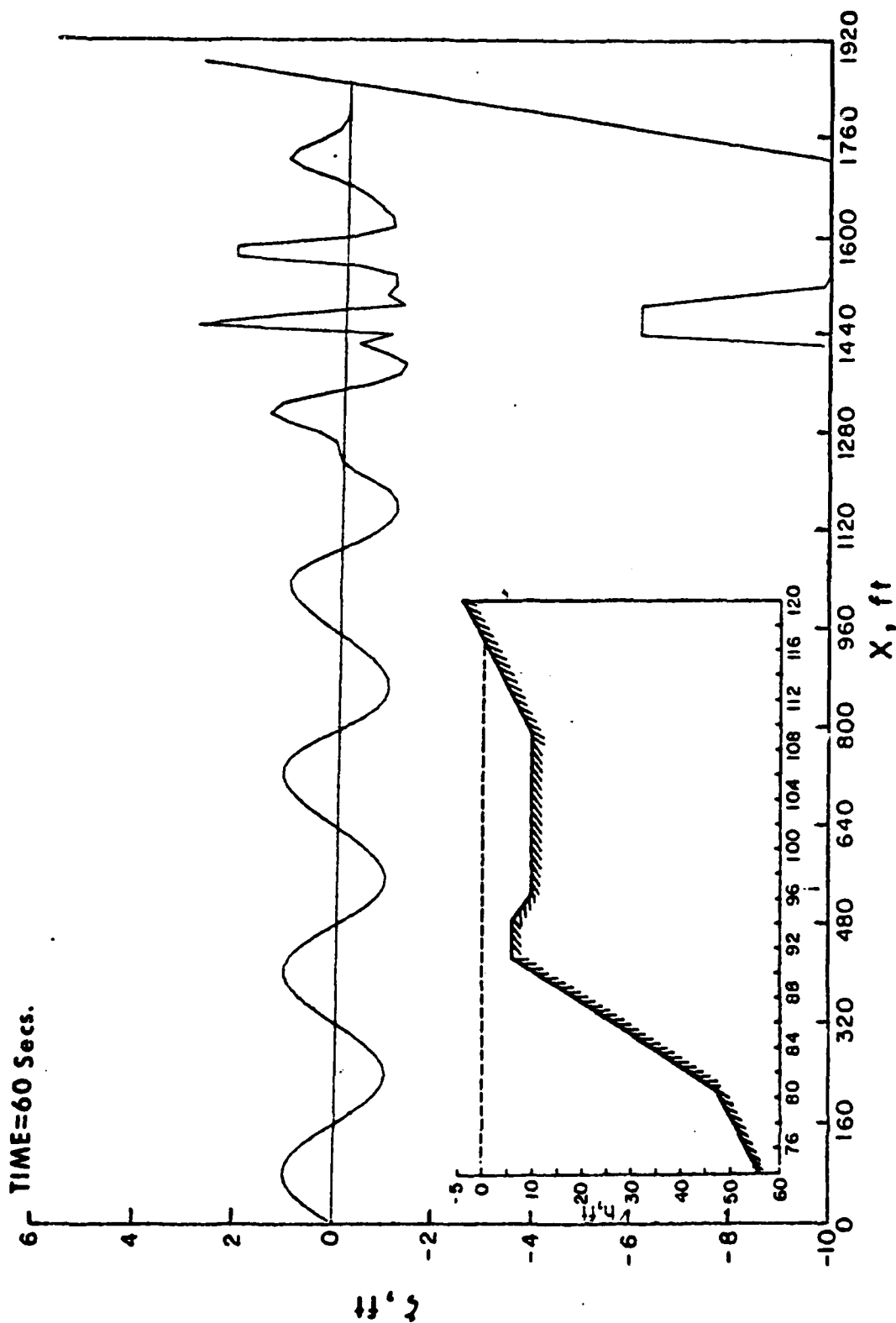
Fig. 11 Beach-With-Bar Wave Profile at 60 Seconds
$\Delta x = 16$ ft., $\Delta t = 0.05$ sec., $n = 0.026$
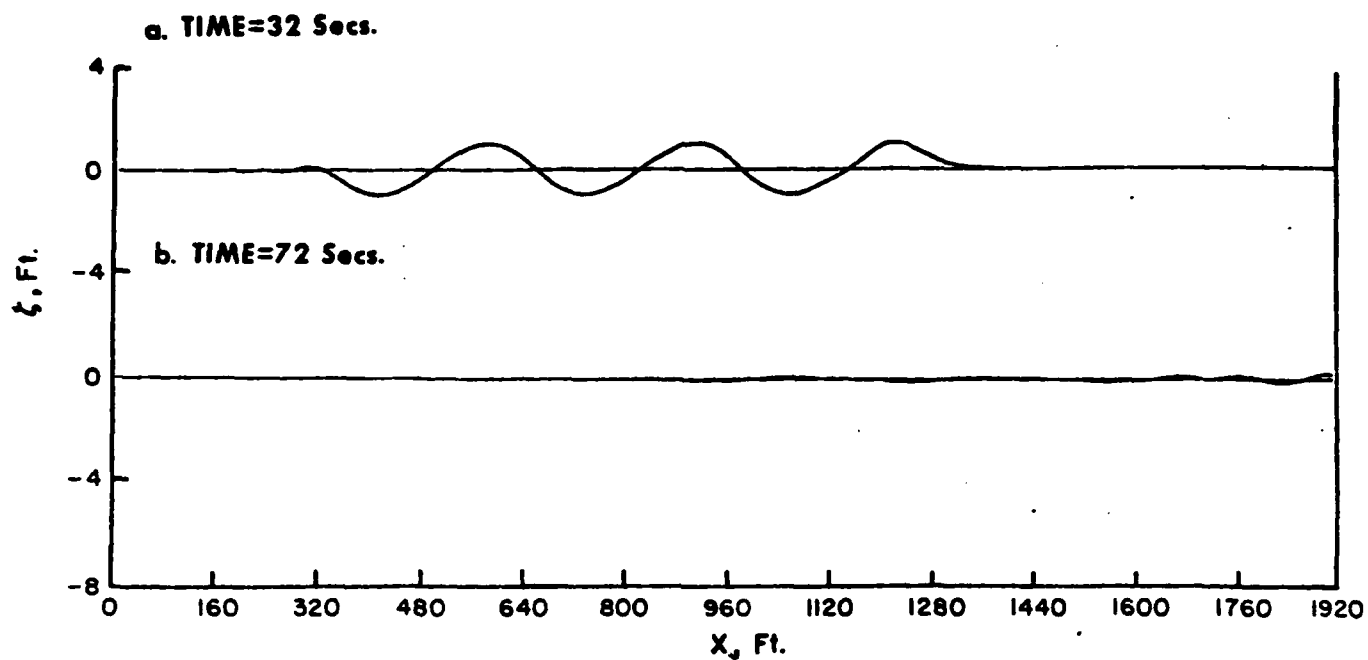
a. TIME=32 Secs.

b. TIME=72 Secs.

Fig. 12 Wave Profiles for Deep Water Configuration (h = 150 ft.)
With Open Downstream Boundary. $\zeta(1,j) = 0, t \geq 24$ sec.
$\Delta x = 16$ ft, $\Delta t = 0.025$ sec, $n = 0.026, \beta = 1$

Fig. 13 Wave Crests at 64 Seconds for the Beach-Breakwater Configuration
$\Delta x = \Delta y = 16$ ft , $\Delta t = 0.2$ sec., n = 0.026

## IV. PREDICTION OF PENETRATION

It is well known that the physical properties of bottom sediments in the coastal zone are highly variable both in space and time. The nature of the bottom sediments; mud, silt, sand, or cemented sediments, can have a large effect on coastal processes, particularly surface waves. The purpose of this effort was to support the Naval Coastal Systems Center in the development of a 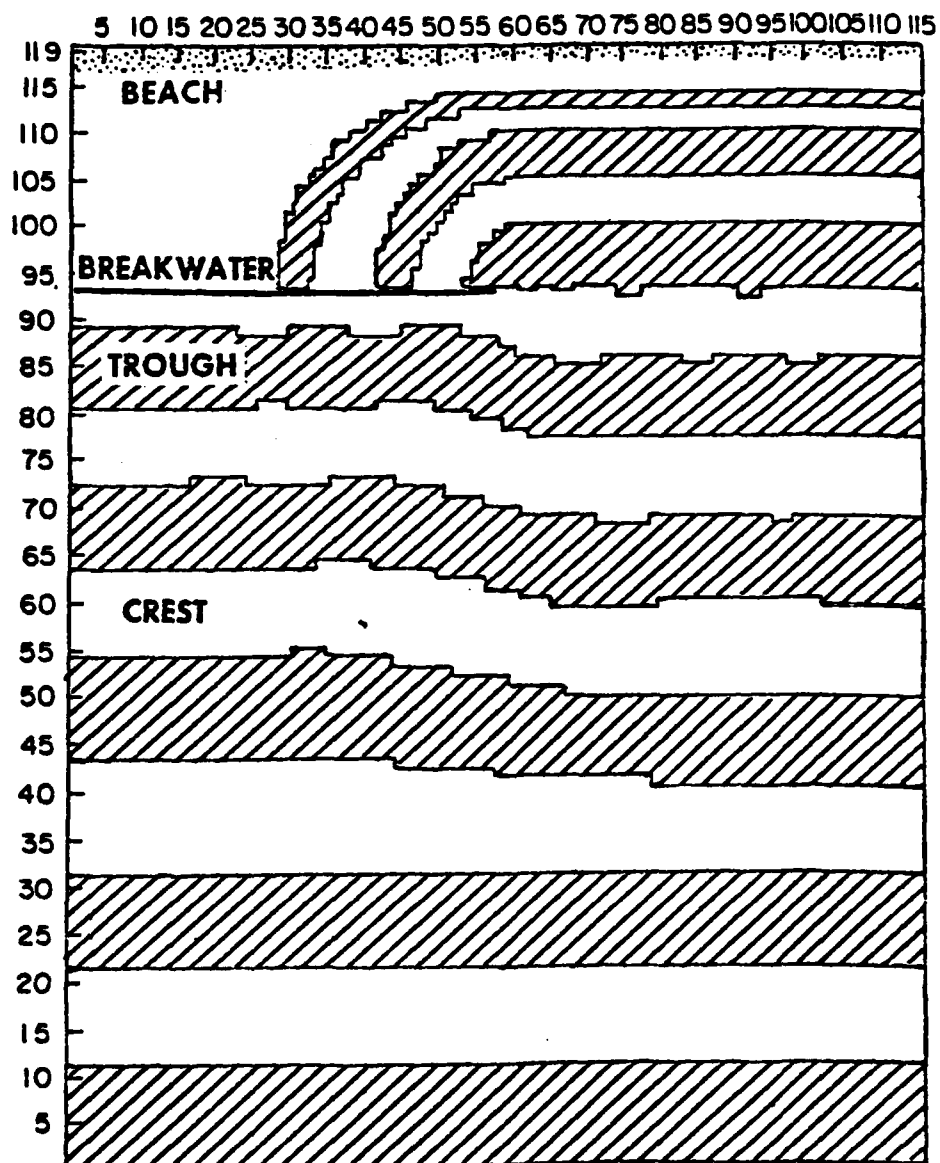technique for rapidly measuring marine sediment properties. One approach that has potential is the instrumented penetrometer (1, 2, 3, 4). The objective of the research was to review existing penetrometer theory and instuments and indicate it's potential for meeting the needs for classifying bottom sediment types.

Recently approaches have been proposed in which soil strength properties can be obtained directly from continuous measurement of cone and sleeve friction. In 1973, (5) experiments were performed in which projectiles were penetrated into kaolin clay targets with known and controlled properties. In their experiments a variety of projectile diameters and weights as well as nose shapes were tested, and it was found that for kaolin clay the side wall resistance is a significant portion of total resistance and that at low velocities the shape of the nose had no effect on the magnitude of side wall resistance. In 1973, (6) a dynamic penetrometer was instrumented with decelerometer, cone and sleeve load cells. Penetration into different type of soils was investigated. This investigation indicated that such an instrument is capable of providing shear strength characteristics of marine sediments. The results of these experiments was that failure mode during impact

penetration is basically of a static nature and cavitation does not occur for impact velocities of less than 19 f/s, and that the friction ratio concept developed from static cone penetration tests for assessing soil types can be extended to impact penetration tests.

The sediment properties which have been related to penetration include sediment type (1, 3), shear strength (2, 4, 5, 6, 7), sensitivity (2, 4), density (2, 4, 5, 6), viscosity (5), shear rate effects (6), and friction angle (7). Typically shear strength values or profiles are determined from either deceleration (2, 3, 4) or tip and sleeve resistance (6, 7).

From a review of present state-of-the-art is feasible to construct an instrumented penetrometer to measure bottom sediment shear strength and classify bottom sediments. The instrumentation would consist of an accelerometer with a range of $\pm 25$ g, a tip resistence gauge with a range up to 1000 Kg and a frictional sleeve gauge with a range up to 750 Kg. The calibration of the penetrometer would initially be done on laboratory samples and then field tested on a variety of sediments. The cost for a research instrument would be in the range of $5,000 to $6,000, an operation system would be less expensive, but a lowest cost figure can't be determined at this time.

1. References

(1) Young, C. W., Depth Prediction for Earth-Penetrating Projectiles, ASCE Proceedings, Vol 95, No. SM3, May, 1969, p. 803-817.

(2) Beard, R. M., Expendable Doppler Penetrometer A Performance Evaluation, Naval Civil Engineering Laboratory, TR-855, July, 1977, 19 pp.

(3)  Young, C. W., Empirical Equations for Predicting Penetration

     Performance in Layered Earth Materials for Complex Penetrator

     Configurations, Sandia Laboratories, SC-DR-720523, December, 1972,

     65 pp.

(4)  McNeill, R. L., Enhancement of Geophysical Soil Profiles using

     Instrumented Marine Sediment Penetrometers, Preprint 3526, Eleventh

     Annual Offshore Technology Conference, Houston, 1979, p. 1469-1480.

(5)  Murff, J., and Coule, H., "Low Velocity Penetration of Keolin

     Clay," Journal of the Soil Mechanics and Foundation Division, ASCE,

     Vol. 99, No. SM5, December, 1971.

(6)  Dayal, Umesh, Allen, John H. and Reddy, Dronnadula V., "Low Veloc-

     ity Projectile Penetration Clay," Journal of the Geotechnical

     Engineering Division, ASCE, Vol. 106, No. GT8, Proc. Paper 15657,

     August, 1980, p. 919-937.

(7)  Arnone, R. A., and L. E. Bowen, Prediction Model of the Time

     History Penetration of a Cylinder through the Air-Water-Sediment

     Phases, Naval Coastal Systems Center, Report 734-36, May, 1980, 55

     pp.

# APPENDIX I

This article is a preprint from the International Ocean Engineering Conference, to be held in Seattle, Washington on September 8-10, 1980. The article indicates the result of field verification of the model under low wave conditions.

# PREDICTING SURF ZONE CONDITIONS FROM AN OFFSHORE BUOY SYSTEM

WALTER W. HOWARD*
JOSEPH N. SUHAYDA**
VERNON W. PIDGEON***

## ABSTRACT

A buoy system and two surf prediction models are
being developed, tested, and evaluated for obtain-
ing wave breaker statistics and longshore currents.
Input data is based upon measurements from an off-
shore location outside the surf zone.

Data from pressure-transducer wave and tide gage,
a two-axes electromagnetic current meter, and
temperature sensors are digitized and sent in a
serial-digital format to an off-line processor.

Both models used to describe the nearshore waves
and longshore current velocity are based upon
linear theory. Results of measurements indicate
that prediction of breaker heights within an
accuracy of 10 to 15 percent is feasible using
offshore measurements.

## INTRODUCTION

The coastal environment plays a key role in many
of the Navy's vital operations. Of specific
interest to the Navy are such parameters as near-
shore waves, tides, currents, and surf conditions.
Actual measurements of these parameters within the
active surf zone is a difficult task, particularly
if it is to be done in a tactical situation. The
surf zone is a very hostile environment on most
occasions. And, it is where the surf is hostile
that information concerning its statistics are
most needed. Measurements outside the surf zone
have been done more extensively and with con-
siderably more success. Also, data processing
techniques have been developed for offshore
conditions as have environmental instrumentation.
Therefore, the use of these developed processes
and hardware coupled together with an effective
reliable prediction, can provide valuable infor-
mation to the coastal investigator.

This paper will report on the efforts of the Naval
Coastal Systems Center (NCSC) to develop an off-
shore buoy system for measuring wave and current
parameters and related prediction models that take
these parameters and generate surf zone statistics,

* Naval Coastal Systems Center, Panama City, FL
** Civil Engineering Dept., Louisiana State
    University, Baton Rouge, LA
*** Dynex Consulting Company, Lynn Haven, FL

The specific details of the buoy system, its appli-
cation, the software algorithms, the data processing,
and test results are given by Pidgeon.[1]

## DATA BUOY SYSTEM

The design of the data buoy system involved con-
siderations of many factors. One of the major
objectives of the design was to develop a measure-
ment system that would operate in shallow water
outside of the surf region and would be able to
measure the hydrodynamic parameters needed as off-
shore inputs into the prediction model for deter-
mining the statistics of wave breakers and the
longshore currents induced by these breakers. A
secondary consideration was the development of a
system that might either lead to or provide signif-
icant information for the design of an operational
buoy system that could be used in Fleet operations
and provide outputs detailing the near-surf and
surf regions of an area under consideration. Al-
though it was realized that this would be a multi-
phase program, ultimate end products were consid-
ered along the various development stages of the
present system. While considerable program devel-
opment was done using the Hewlett Packard HP-9825
programmable calculator, additional processing was
done using microcomputers in preparation for adap-
ting the buoy system to perform on-board data
processing utilizing state-of-the-art micropro-
cessing components within the buoy.

The buoy system measures waves, tides, two or-
thogonal components (horizontal) of current, water
temperature, internal temperature, and system
calibration. Waves and tides are simultaneously
measured by a Statham, Model UC-3, pressure cell.
A Marsh-McBirney, Model 711, two-axis electro-
magnetic induction current meter measures water
motion in the horizontal plane. Water temperature
is measured both inside and outside the unit by
using two Analog Devices, Model AD590, two-terminal
integrated circuit temperature transducers. In
addition, a leak detector circuit was added to the
buoy to detect the presence of water in the bottom
of the unit. All signal outputs from the system
sensors are analog voltages and are tied into a
16-channel analog to digital multiplexer having
12-bit accuracy prior to transmission to shore.
The sensors and all associated electronics are
contained in a cylindrical pressure housing capable
of withstanding pressures equivalent to 30 meters of
water depth. Weighing less than 25 kilograms in
air, the buoy is easily deployed by divers and is
normally attached to a stand that has been previ-
ously jetted into the bottom for support.

A major consideration in the design of the buoy system was the method of getting the analog signals from the sensors to the processing equipment. Desirably, the data would be sent in digital form in order to obtain the most immunity from noise and other degrading factors. Also, in order to avoid having many signal lines between the buoy and the receiving station, a serial not a parallel system was needed. A very important consideration in the design of this interfacing system was the formatting and makeup of the data. With future on-board processing in mind, a format that would be directly compatible with mocrocomputers and other similar processors is what is needed. Each of these considerations fit very well into an interfacing system that has been developed by Dynex for another NCSC task. This system, called Information Transmission System (ITS)[2], takes multiple analog data channels (up to 128), multiplexes them into a 12-bit digitizer (giving one millivolt resolution out of four volts), converts the parallel output data into two eight-bit bytes, which are sequentially applied to a standard UART (Universal Asynchronous Receiver Transmitter), from which the data are sent in a bit-serial, digital format. The serial format is completely compatible with computer standards for serial data transfer, i.e., meets RS-232C standards. Therefore, any computer processor with a standard RS-232 serial interface can accept the data from this buoy system without any further modification.

An important consideration in the transfer of data from the measuring source to the processing system is the preservation of the data as nearly as measured as practical. Secondly, the ability to input directly into the processor with minimal reformatting means more efficiency, fewer errors, and less processing costs. For on-board processing, both of these considerations are almost mandatory. These factors are the prime ones considered in the development of the ITS system, and they also made it a prime candidate for the data buoy system. The addition of ITS to the buoy system allowed considerable flexibility in how the data could be handled, once it was obtained in the buoy. The data could be transmitted via standard telemetry links with relatively low bandwidths. Or the data could be directly connected to a beach site via cable. This latter version was selected for these preliminary tests since both data signals and buoy power could be cabled between the beach site and the buoy with a modest cable having as few as four conductors—two for power and two for signals.

Since it was desirable to record data at selected intervals, it was decided to input the data signals directly from the buoy cable into a standard Bell 103 telephone modem, having an auto-answer capability. The RS-232 data format at a 300 baud rate is completely compatible with this type modem. Thus, when it was desired to take data or to check the buoy operation, all that one had to do was to call up the buoy from NCSC or the Dynex office with either an acoustic coupler (which was used by NCSC) or a modem (which was used by Dynex). When the

modem at the beach tower auto-answered, the handshake was completed at the originating end. At this point, data began to stream in and continued until the originating source turned off its lockup tone or the calling phone was hung-up. The data that was received could then be used in several ways. It could be checked to ascertain proper buoy operation, it could be used to determine the real-time conditions of the Gulf of Mexico at that time, or it could be directly recorded or input into the processor for data processing.

In order to be able to sample the wave data rapidly enough to detail with accuracy the wave profile, the wave data were sampled most often of the data. This was done by putting the wave data on every other channel. Interdispersed beween the wave data were the other signals. With the ITS system running at 300 baud wave data were sampled almost five times per second. This was sufficiently fast enough to adequately determine wave shape. (It is necessary in the data processing to determine the peak and trough of each individual wave as well as its period. Therefore, an accurate reproduction of the wave profile is necessary.)

## PREDICTIVE MODELS

Using the wave buoy to provide a time history of hydrodynamic pressure and the two horizontal components of water motion at a point seaward of the surf zone, a scheme was developed to compute the following parameters:

a) Average breaker height ($\bar{H}$) and maximun breaker height ($H_m$)

b) Average breaker position ($\bar{X}$) and maximum breaker position ($X_m$)

c) Breaker type (i.e., plunging, spilling or surging)

d) Average longshore current ($\bar{V}_1$) and maximum longshore current ($V_{1m}$)

Wave theory used for this study is linear wave theory. This theory is able to treat waves in intermediate and shallow water and is easily programmable onto a microcomputer. It is, of course, limited to waves of small height to wave length ratios (low steepness), and small wave height to water depth ratios. In addition to wave and current parameters, bottom slope ($\beta$), elevation of buoy off the bottom ($d_1$) and orientation of current meter (y-axis, parallel to shoreline and x-axis, normal to shoreline) are also required input parameters (see Figure 1). Data is sampled at a constant time interval, $\Delta t$, over an interval of time, t, to produce N data samples, where N equals $t/\Delta t$. Usually t will be in the range of five to 20 minutes and $\Delta t$ will be 0.25 to one second.

## PRELIMINARY COMPUTATIONS

The preliminary computations include determining the mean pressure ($\bar{P}$), the pressure change between wave crest and wave through for each wave ($\Delta P$; $j=1 \cdots M$), the wave period for each wave ($T$), the mean velocity components ($\bar{V}$ and $\bar{U}$) and the wave crest current components ($U_{cj}$ and $V_{cj}$).

The wave parameters computed for the location of the instrument are:

water depth $\quad h = \dfrac{\bar{P}}{\rho g} + di$

and for each wave:

wave height $\quad H_j = \dfrac{\Delta P_j}{\rho g} \dfrac{\text{COSH} \ (2\pi h/L_j)}{\text{COSH} \ (2\pi di/L_j)}$

wave length $\quad \dfrac{2\pi}{T_j} = \dfrac{2\pi g}{L_j} \text{TANH} \ (2\pi h/L_j)$

Wave angle $\quad \theta_j = \text{TAN}^{-1} \ \dfrac{(V_{cj})}{(U_{cj})}$

## SIMPLIFIED MODEL-PREDICTION EQUATIONS

For the prediction of breaker heights, the simplified model utilizes pressure measurements (uncorrected for the depth) from the bottom mounted pressure transducer and computes a breaker height from the following equation:

$$H_b = \left[ .89 \ \frac{\bar{P}}{\rho g} + h_1 \ \left(\frac{\Delta P}{\rho g}\right)^4 \right]^{1/5}$$

This computation is made for each individually measured wave recorded at the data buoy.

The predictive model also gives a prediction of the maximum longshore current from the measured average longshore current at the buoy and the predicted breaker depth obtained from the mean breaker height as given by:

$$V_{1m} = 1.7 \bar{V} \ \left(\frac{H}{h_b}\right)^4$$

## DETAILED MODEL-PREDICTION EQUATIONS

The prediction of the surf zone parameters involves a set of equations which must be applied simultaneously. The equations use the instrument site wave parameters $H_j$, $T_j$, $L_j$, and $\theta_j$ to predict the same parameters at the break point $H_b$, $T_b$, $L_b$, $\theta_b$. It is assumed that the period of each wave remains constant so that $T_j = T_{bj}$. The equations are as follows (3):

1) **Breaker Depth**

$$h_{bj} = H_{bj} \ (1-4.7\beta + 12\beta^2), \quad \beta \le .15$$

2) **Breaker Angle**

$$\text{SIN} \ \theta_{bj} = \frac{C_{bj}}{C_j} \ \text{SIN} \ \theta_j$$

$$C_j = \frac{L_j}{T_j}, \quad C_{bj} = [g(H_{bj}+h_{bj})]^{\frac{1}{2}}$$

3) **Breaker Wavelength**

$$L_{bj} = C_{bj} \cdot T_j$$

4) **Breaker Height**

$$H_{bj} = H_j \cdot K_{rj} \cdot K_{sj} \cdot K_{fj}$$

where

$$K_{fj} = .98, \quad K_{rj} = \left[\frac{\text{COS}\theta_j}{\text{COS}\theta_{bj}}\right]^{\frac{1}{2}}$$

$$K_{sj} = \left[\frac{\text{TANH} \ (2\pi h/L_j)}{\text{TANH}(2\pi h_{bj}/L_{bj})}\right] \cdot \left[\frac{1 + \dfrac{4\pi h/L_j}{\text{SINH}(4\pi h/L_j)}}{1 + \dfrac{4\pi h_{bj}/L_{bj}}{\text{SINH}(4\pi h_{bj}/L_{bj})}}\right]^{1/2}$$

The set of breaker values are computed for $j = 1 \cdots M$. For this the maximum breaker height $H_m$ can be identified, furthermore

$$\bar{H}_b = \frac{1}{M} \sum_{j=1}^{M} H_{bj}, \quad \bar{h}_b = \frac{1}{M} \sum_{j=1}^{M} h_{bj}$$

$$\bar{\theta}_b = \frac{1}{M} \sum_{j=1}^{M} \theta_{bj}$$

The positions of $\bar{h}_b$ and $h_{max}$ can be located on the nearshore chart.

## PREDICTION PROCEDURE-DETAILED MODEL

The simultaneous solution of the set of equations needed to make a prediction is too complex for a practical scheme. Rather, the solution can be approximated by an iteration scheme in which initial values for selected parameters are computed from an input data. The formula for the initial value of the wave height is

$$H^*_{bj} = .95 \ h^{1/5} \ H_j^{4/5}$$

With this initial value, the set of equations in the surf prediction model can be computed explicitely in order, that is, finding $h_{bj}$, use this to fi... $_{bj}$ and finally $H_{bj}$. The difference between $H_{bj}$ and $H^*_{bj}$ should be small ( a few percent) and, if not, $H_{bj}$ can be used in place of $H^*_{bj}$ in a second iteration.

## BREAKER TYPE

The prediction of breaker type is based upon breaker wave characteristics and the beach slope. The empirical formula suggested is:

$$\frac{H_{bj}}{L_{bj} \cdot \beta} > 1.2 \text{ SPILLING BREAKER}$$

$$.5 \leq \frac{H_{bj}}{L_{bj} \cdot \beta} \leq 1.2 \text{ PLUNGING BREAKER}$$

$$\frac{H_{bj}}{L_{bj} \cdot \beta} < .5 \text{ SURGING BREAKER}$$

## LONGSHORE CURRENT MODEL

The prediction of longshore currents is based upon the theory of linear waves on a plane sloping beach. The formula for the maximum longshore current $V_m$ and the longshore current at the average point $V_b$ are given by (4):

$$V_m = 20.7 \cdot \beta (g\bar{H}_b)^{\frac{1}{2}} \text{ SIN } 2\bar{\theta}_b$$

and

$$V_b = .60 \ V_m$$

## FIELD TESTS AND RESULTS

To date the buoy has been deployed on five different occasions to acquire data for various sea state conditions. Prior to each deployment and upon return to NCSC, the entire system undergoes a check procedure to verify operability and calibration. Problems encountered with the use of a cable between buoy site and shore station have been the most prevalent. Strong longshore currents associated with the passage of storm fronts have caused the cable to break or to pull away from the buoy on several different occasions.

To properly evaluate the predictive models, it was desired to compare actual measurements of breaker heights on an individual basis with corresponding predicted heights. This necessitates time correlation of recorded buoy measurements with observed/ measured breaker measurements. Due to the dispersive nature of waves approaching the breaking zone, the sequence of waves arriving at the buoy will not necessarily be the same sequence that arrive at the breaker zone. However, in general, the measurements of a group of waves can be compared with that

for time-delayed measurements to the breaker region for a similar group of breakers.

Two different approaches to the verification of the predicted heights were utilized. The first approach developed was a technique using a transit with vertical graduations. This vertical scale was calibrated for known locations (anchored floats) within the breaking zone. Vertical displacement of the float was measured, giving a reasonably accurate measurement of waves immediately prior to breaking. A comparison of measured versus predicted breaker heights for the predictive models is presented in Table 1. Although it was not possible to make a one-for-one comparison between the predicted breaker heights and the measured breaker heights, their respective statistics provided adequate data for comparison.

It can be observed that the detailed model over-predicts the heights in all cases, whereas the simplified model comes closer to the measured conditions, in some cases under-predicting, but in others over-predicting. However, on the average, the simplified model is very close except for the largest of the heights. For this test date the average wave periods are running close to six seconds. It should be noted that periods of less than three seconds are not included due to frequency cut-off of pressure transducer.

A brief examination of the effect of beach slope on the results given for the detailed model was done. A slope of 1:20 was used for the data processing. At this point, this value is felt to be too large. 1:30 to 1:50 probably fits the conditions more closely. Using the more gradual slope in the detailed model, the prediction results for the cases tested was less, but not by as much as the results for this test date indicate. The slope, as well as other factors, need to be further investigated for model refinement.

It should be noted at this point, that the results of the comparisons of the models with observations are very encouraging. The results indicate that for breaker heights up to two meters, the detailed model predicts breaker heights to an accuracy of the order of ten percent. For the higher energy waves, the simplified model does almost as well, but does less well for the shorter wave periods with lower amplitudes.

The second approach to model verification involves the use of wave data collected from the U. S. Army Coastal Engineering Research Center Field Research Facility at Duck, North Carolina. Breaking wave data recorded from a series of wave gages positioned throughout the active surf zone will be compared with predicted breaker heights whose input data have been simultaneously recorded from gages positioned just outside the surf zone. These detailed time correlated measurements will provide valuable calibration data for both predictive models. Results of this experiment will be published at a later date.

## CONCLUSIONS

Regarding the over-all buoy system and its operation, the results of this study have demonstrated that this system is a very reliable one, has the ability to measure very accurately the required wave, tide, and current inputs for data processing, is easily deployable by divers from a small boat with minimum equipment required, and is readily adaptable to a variety of Fleet operations and applications. It has demonstrated that it can withstand the hostile environment of the near-surf zone within the limits tested and has the ability to transmit its data via a wide variety of methods to the end user, thus making this buoy system a prime candidate for Fleet operations.

The models presented in this study provide a means for making predictions of the desired surf parameters. Each model is limited in application because of the assumptions contained in the underlying wave theory. The models do not account for wave induced pressures near the break point, resulting from wave crest accelerations. Furthermore, the bottom topography is assumed to be planar and therefore real beach profiles and longshore bars cannot be treated. Finally, the longshore current predictions neglect temporal variations in current speed and spatial variations associated with near-shore topography.

It is concluded that the software developed for the support operations of the buoy system is efficient in terms of processing capabilities of speed, size, and complexity, can be adapted to on-board buoy processing without considerable modification, is flexible and readily adaptable to a wide range of user applications, and the study results further show the software to be reliable and accurate.

It is further concluded that both of the prediction models used in this study give very good results, often with prediction errors of only a few percent, that the detailed model allows for a greater flexibility and range of environmental inputs but does require more complexity in processing, and that the simplified model, although limited, gave accuracies that are well within the requirements of many user applications.

### ACKNOWLEDGMENTS

TABLE 1. COMPARISON OF MEASURED VERSUS PREDICTED BREAKER HEIGHTS FOR SIMPLIFIED AND DETAILED MODELS TEST DATE 7 DECEMBER 1979

| TIME | AVERAGE BREAKER HEIGHT (M) | | |
|---|---|---|---|
| | Simpl. Model | Detail Model | Meas'd |
| 11:15–11:18 | .69 | .83 | |
| 11:18–11:22 | .70 | .81 | |
| 11:22–11:26 | .76 | .85 | |
| AVERAGE 11:15–11:26 | .72 | .82 | .73 |
| 11:28–11:31 | .69 | .83 | |
| 11:31–11:35 | .79 | .86 | |
| 11:35–11:39 | .75 | .84 | |
| AVERAGE 11:28–11:39 | .74 | .84 | .76 |
| AVERAGE ALL TIMES 11:15–11:39 | .73 | .83 | .75 |

| TIME | AVERAGE HIGHEST 1/3 (M) | | |
|---|---|---|---|
| | Simpl. Model | Detail Model | Meas'd |
| 11:15–11:18 | .98 | 1.19 | |
| 11:18–11:22 | .96 | 1.06 | |
| 11:22–11:26 | 1.01 | 1.04 | |
| AVERAGE 11:15–11:26 | .98 | 1.08 | 1.07 |
| 11:28–11:31 | 1.02 | 1.07 | |
| 11:31–11:35 | 1.12 | 1.13 | |
| 11:35–11:39 | 1.01 | 1.02 | |
| AVERAGE 11:29–11:39 | 1.05 | 1.07 | .98 |
| AVERAGE ALL TIMES 11:15–11:39 | 1.02 | 1.08 | 1.03 |

| TIME | AVERAGE HIGHEST 1/10 (M) | | |
| --- | --- | --- | --- |
| | Simpl. Model | Detail Model | Meas'd |
| 11:15-11:18 | 1.14 | 1.29 | |
| 11:18-11:22 | 1.09 | 1.22 | |
| 11:22-11:26 | 1.36 | 1.37 | |
| AVERAGE 11:15-11:26 | 1.19 | 1.29 | 1.13 |
| 11:28-11:31 | 1.24 | 1.25 | |
| 11:31-11:35 | 1.23 | 1.23 | |
| 11:35-11:39 | 1.12 | 1.24 | |
| AVERAGE 11:29-11:39 | 1.20 | 1.21 | 1.08 |
| AVERAGE ALL TIMES 11:15-11:39 | 1.20 | 1.25 | 1.10 |

REFERENCES

1. Pidgeon, V.W. and N.A. Pidgeon, "An Environmental Data Buoy System for Predicting Surf-Zone Characteristics," Dynex Consulting Company, Report, FR-XX-1, February 29, 1980.

2. Pidgeon, V.W. and N.A. Pidgeon, "A Development Study for a Field and Laboratory Data System," Dynex Consulting Company Report, FR,XVI-2, November 1, 1979.

3. U. S. Army Corps of Engineers Coastal Engineering Research Center, Shore Protection Manual, Vols. I, II, and III, 1973.

4. Lonquet-Higgens, M.S., "Longshore Currents Generated by Obliquely Incident Sea Waves, 1," Jours. Geographical Res., Vol 75, 6778-6789, 1970.
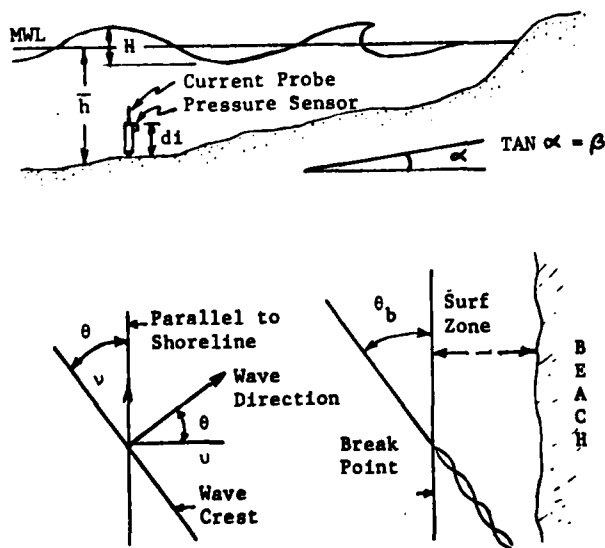
FIGURE 1. Schematic Diagram of Beach and Definition of Variables.

# DISTRIBUTION LIST

| | |
|---|---|
| Office of Naval Research<br>Coastal Sciences Program<br>Code 422CS<br>Arlington, VA 22217 | 3 copies |
| Defense Documentation Center<br>Cameron Station<br>Alexandria, VA 22314 | 12 copies |
| Director<br>Naval Research Laboratory<br>ATTN: Technical Information Officer<br>Washington, D.C. 20375 | 3 copies |
| Director<br>Office of Naval Research Branch<br>  Office<br>1030 East Green Street<br>Pasadena, CA 91101 | 1 copy |
| Commanding Officer<br>Office of Naval Research Eastern/<br>  Central Regional Office<br>Building 114, Section D<br>666 Summer Street<br>Boston, MA 02210 | 1 copy |
| Office of Naval Research<br>Code 422PO<br>National Space Technology<br>  Laboratories<br>Bay St. Louis, MS 39529 | 1 copy |
| Office of Naval Research<br>Code 422PO<br>Washington, D.C. 22217 | 1 copy |
| Office of Naval Research<br>Code 100M<br>Washington, D.C. 22217 | 1 copy |
| Office of Naval Research<br>Operational Applications Division<br>Code 200<br>Arlington, VA 22217 | 1 copy |
| Commander<br>Naval Oceanographic Office<br>ATTN: Library, Code 1600<br>NSTL Station, MS 39529 | 1 copy |

Commander                                          1 copy
Naval Coastal Systems Center
ATTN: Library, Code 116.1
Panama City, Florida  32401

Librarian                                          1 copy
Naval Intelligence
Support Center
4301 Suitland Road
Washington, D.C.  20390

Officer in Charge                                  1 copy
Environmental Prediction
Research Facility
Naval Post Graduate School
Monterey, CA  93940

Director                                           1 copy
Amphibious Warfare Board
U.S. Atlantic Fleet
Naval Amphibious Base
Norfolk, Little Creek, VA  23520

Commander                                          1 copy
Amphibious Force
U.S. Pacific Fleet
Force Meteorologist
Comphibpac Code 255
San Diego, CA  92155

Commanding General                                 1 copy
Marine Corps Development and
  Educational Command
Quantico, VA  22134

Chief of Naval Operations                          1 copy
OP 987J
Department of the Navy
Washington, D.C.  20350

Commandant                                         1 copy
U.S. Coast Guard
ATTN: GECV/61
Washington, D.C.  20591

National Oceanographic Data Center (D764)    1 copy
Environmental Data Services
NOAA
Washington, D.C.  20235

Defense Intelligence Agency                        1 copy
Central Reference Division
Code RDS-3
Washington, D.C.  20301

Central Intelligence Agency                1 copy
ATTN:  OCR/DD-Publications
Washington, D.C.  20505.

Director                                   1 copy
Coastal Engineering Research Center
U.S. Army Corps of Engineers
Kingman Building
Fort Belvior, VA   22060

DATE
FILMED

2-8